Geotechnique

Foundation punch-through in clay with sand: centrifuge modelling

--Manuscript Draft--

Manuscript Number:	16-P-100R3
Full Title:	Foundation punch-through in clay with sand: centrifuge modelling
Article Type:	General Paper
Corresponding Author:	Shah Neyamat Ullah, PhD National University of Singapore Singapore, SINGAPORE
Corresponding Author's Institution:	National University of Singapore
Order of Authors:	Shah Neyamat Ullah, PhD
	Samuel Stanier, PhD
	Yuxia Hu, PhD
	David White, PhD
Corresponding Author's Secondary Institution:	
Order of Authors Secondary Information:	
Manuscript Region of Origin:	AUSTRALIA
Abstract:	This paper is concerned with the vertical penetration resistance of conical spudcan and flat footings in layered soils. Centrifuge tests are reported for a clay bed with strength increasing with depth interbedded with dense and medium dense sand. Both non-visualising (full-model) and visualising (half-model) tests were conducted with high quality digital images captured and analysed using the PIV (particle image velocimetry) technique for the latter. The load displacement curves often show a reduction in resistance on passing through the sand layers, which creates a risk of punch-through failure for the foundations when supporting a jack-up drilling unit. For a given foundation, the peak punch through capacity (qpeak) is dependent on the thickness of both the overlying clay and the sand layer. The failure mechanism associated with the peak resistance in the sand layer involves entrapment of a thin band of top clay above the sand layer that subsequently shears along an inclined failure surface before being pushed into the underlying clay. The top clay height when normalised by the foundation diameter affects the soil failure pattern in this layer and along with the sand layer thickness controls the severity of the punch-through failure (i.e. the additional penetration before the resistance returns to the peak value). Comparisons are made with current industry guidelines for predicting qpeak and the risk of punch through failure for sand-overlying clay. These methods are shown to be conservative in their prediction of qpeak but inconsistent in predicting punch-through.
Suggested Reviewers:	
Opposed Reviewers:	
Additional Information:	
Question	**Response**
Please enter the total number of words in the main text only. The main text of the paper should be as concise as possible. The word count of General Papers should not exceed 5000 words and for Technical Notes should not exceed 2000 words. The word count of a submission excludes	6109

the abstract, list of notation, acknowledgements, references, tables and figure captions. Discussions, Book Reviews, and Obituaries should be less than 1000 words. Whilst Geotechnique reserves the right to publish papers of any length Authors should be aware that any submission for a General Paper that is significantly over the word limit will be subjected to pre-assessment and may be returned to the Authors for editing prior to being sent for review. The word limit for Technical Notes will be strictly adhered to, and if over 2000 words, the submission will be considered as a General Paper.	
Have you included a full notation list including definitions (and SI units of measurement where appropriate) for any mathematical terms and equations included in your paper?	Yes
Have you included a completed copyright transfer form? This is required for all publications and can be found here.	Yes
Have you uploaded each of your figures separately and in high-resolution .tiff (ideal for photographs) or .eps files (best for line drawings)? This is required for all figures before your paper can be accepted. Our figure requirements can be found here.	Yes
Have you uploaded your tables in an editable Microsoft Word (.doc) format?	Yes
Have you included a separate list of all your figure and table captions?	Yes
Are your figures clear when printed in black and white? (For example, are plot lines distinguishable; are tints sequentially graded?) As this journal is printed in black and white, any figures that are unclear may be removed.	Yes
Are your references in Harvard style? Our reference guidelines can be found here.	Yes
To ensure your paper is indexed correctly – and therefore as discoverable as possible – in our ICE Virtual Library, please choose up to 6 keywords from our Keywords List. This can be found here. We are unable to accept keywords that do not appear on this list.	Bearing capacity,Centrifuge modelling,Offshore engineering, Soil/structure interaction, Footings/foundations, Model tests
Manuscript Classifications:	Centrifuge; COASTAL, MARINE AND OFFSHORE GEOTECHNICS; Offshore foundations; PHYSICAL MODELLING; Spudcan foundations
Author Comments:	

Date of Writing-13/04/2016

Title of Submission- Foundation punch-through in clay with sand: centrifuge modelling

Authors:

i) Shah Neyamat Ullah (contact author)

PhD

Research Fellow

National University of Singapore

Former PhD student

Centre for Offshore Foundation Systems

University of Western Australia, Crawley, WA 6009, Australia.

(Telephone +65 9814 2663; Email: shahneyamat.ullah@nus.edu.sg)

ii) Samuel Stanier

PhD

Research Fellow, Centre for Offshore Foundation Systems

University of Western Australia, Crawley, WA 6009, Australia.

Email: sam.stanier@uwa.edu.au

iii) Yuxia Hu

PhD

Professor, School of Civil, Resource and Mining Engineering

University of Western Australia, Crawley, WA 6009, Australia.

Email: yuxia.hu@uwa.edu.au

iv) David White

PhD

Winthrop Professor, Centre for Offshore Foundation Systems

University of Western Australia, Crawley, WA 6009, Australia.

Email: david.white@uwa.edu.au

Words: Main text = 6109; Abstract = 242;

Figures: 16

Tables: 2

FOUNDATION PUNCH- THROUGH IN CLAY WITH SAND: CENTRIFUGE MODELLING

Shah Neyamat Ullah, Samuel Stanier, Yuxia Hu & David White

ABSTRACT

This paper is concerned with the vertical penetration resistance of conical spudcan and flat footings in layered soils. Centrifuge tests are reported for a clay bed with strength increasing with depth interbedded with dense and medium dense sand. Both non-visualising (full-model) and visualising (half-model) tests were conducted with high quality digital images captured and analysed using the PIV (particle image velocimetry) technique for the latter. The load displacement curves often show a reduction in resistance on passing through the sand layers, which creates a risk of punch-through failure for the foundations when supporting a jack-up drilling unit. For a given foundation, the peak punch through capacity (q_{peak}) is dependent on the thickness of both the overlying clay and the sand layer. The failure mechanism associated with the peak resistance in the sand layer involves entrapment of a thin band of top clay above the sand layer that subsequently shears along an inclined failure surface before being pushed into the underlying clay. The top clay height when normalised by the foundation diameter affects the soil failure pattern in this layer and along with the sand layer thickness controls the severity of the punch-through failure (i.e. the additional penetration before the resistance returns to the peak value). Comparisons are made with current industry guidelines for predicting q_{peak} and the risk of punch through failure for sand-overlying clay. These methods are shown to be conservative in their prediction of q_{peak} but inconsistent in predicting punch-through.

INTRODUCTION

Jack-up rigs are commonly deployed in water depths of up to 150 m for extraction of hydrocarbons via drilling. The foundations of these jack-up rigs are penetrated into the seabed under water ballast preload to embed the foundations and improve their fixity prior to operation. During preloading punch-through can occur when a soft soil layer (such as soft clay) is overlain by a thin strong layer (such as dense sand or stiff clay) resulting in a rapid plunging of the foundation (e.g. Baglioni *et al*., 1982). A comprehensive historical account (1957-2002) of jack-up foundation failures was given by Dier *et al*. (2004), and concluded that more than 50% of failures are associated with punch-through.

Punch-through has been the subject of extensive research in recent years. The soil stratigraphies that display the potential for punch-through include: (i) sand-clay stratigraphies (Teh *et al*., 2010; Lee *et al*., 2013a; Hu *et al*., 2014a); (ii) clay stratigraphies following a period of sustained preloading (Bienen and Cassidy, 2013; Stanier *et al*., 2014; Bienen *et al*., 2015); and (iii) interbedded clay layers (Hossain *et al*., 2011). Multi-layer deposits with interbedded sand are also common in regions with offshore hydrocarbon reserves, such as the Gulf of Suez, Southeast Asia, Gulf of Mexico and offshore South America (Baglioni *et al*., 1982; Dutt & Ingram, 1984; Teh *et al*., 2009). Figure 1 shows offshore borehole logs of clay stratigraphies with interbedded sand from the Gulf of Suez (Figure 1 a) and Gulf of Mexico (Figure 1 b) that could result in punch-through.

Research into the potential for punch-through at clay-sand-clay sites has been limited. (Hossain, 2014) recently reported a small number of experiments on clay-sand-clay stratigraphies. This paper reports two comprehensive sets of experiments – visualising (i.e. half-model PIV tests performed against a transparent window) and non-visualising (i.e. full-model penetration tests) – that were performed in a drum centrifuge. Both conical spudcan and flat foundation shapes were tested for a range of clay-sand-clay stratigraphy geometries (varying clay and sand layer heights) and a range of material properties (including sand relative density and clay shear strength). High quality digital images captured during the visualising experiments have been analysed using the Particle Image Velocimetry (PIV) technique (e.g. White *et al*., 2003) allowing identification of the soil flow mechanisms at various key stages of the penetration process. Finally, the performance of the current industry guideline (SNAME, 2008; ISO, 2012) in predicting (i) the peak penetration resistance in the sand layer, (ii) the bearing capacity in the underlying clay layer and (iii) the maximum punch-through distance is assessed. While this paper reports the experimental findings, the companion paper develops an analytical model for prediction of the load-penetration response in sand-clay and clay-sand-clay stratigraphies (Ullah *et al.* 2016a).

EXPERIMENTAL DETAILS

Centrifuge apparatus

The drum centrifuge at UWA (described by Stewart *et al.* 1998) was used for all of the experiments reported. Visualising experiments were performed in strongboxes 180 mm (radial depth) by 258 mm (length) by 80 mm (width) in size, which were located and observed within the centrifuge channel using the system described by Stanier & White (2013). Non-visualising experiments were performed within the drum centrifuge channel, which is 300 mm (width) by 200 mm (radial depth). All experiments were performed at an acceleration of 200g (where g is earth's gravity).

Soil sample preparation

Commercially available kaolin clay powder and superfine silica sand were used in all of the experiments. The relevant engineering properties are reported by Lee *et al*., 2013a. Particle size distributions can be found for these two materials in Xu (2007). The soil samples were created using a multi-stage process. First, clay slurry was mixed to approximately twice its liquid limit and poured into the drum centrifuge strongbox or channel (for visualising and non-visualising tests respectively) in-flight, at an acceleration of 20g. The clay was subsequently consolidated at 300g with periodic top-ups of further slurry, resulting in a bed of normally consolidated clay ~170 mm deep in case of the non-visualising tests and ~140 mm in the visualising tests. The upper layer of clay was removed from the sample leaving approximately 80 mm and 120 mm of clay in the strongboxes and centrifuge channel respectively.

For the visualising experiments performed in the strongbox, sand was pluviated into the strongbox at 1g. The sand layer was scraped flat to achieve the desired sand layer height, following which a part of the clay layer previously removed was placed back to achieve the desired clay layer height. To provide additional image texture for the PIV analyses, coloured modelling flock was sprinkled uniformly onto the exposed plane of the model using a sieve after careful removal of the transparent window. The density of this modelling flock was optimised by matching it to that identified for the optimal Artificial Seeding Ratio (ASR) following the procedure proposed by Stanier & White, (2013). Different colour modelling flock was used for the sand and clay layers to distinguish them in the images captured.

For the non-visualising full drum channel experiments superfine silica sand was air-pluviated in-flight through a layer of surface water in the channel onto a porous fabric filter placed on top of the clay sample. The pluviation nozzle and sand particle falling height were controlled to achieve the desired relative density (I_D) of the sand layer (i.e. larger nozzles and lower fall heights lead to looser sand layers). The sample was spun for a further period at 200g to allow the sand layer to settle and the underlying clay layer to consolidate further. Cracking in the surface of the sand layer was observed due to the increase in circumference of the sand surface caused by its settlement in the channel. Thus, after the completion of consolidation, the original sand layer and porous fabric filter were removed and a new sand layer was pluviated into the channel directly onto the consolidated clay. The sand surface was then scraped radially using a thin aluminium sheet to achieve the first target sand layer height. After this an overlying clay layer was created by pouring more clay slurry into the centrifuge channel in-flight for the non-visualising experiments. Following consolidation of the top clay layer, the sample surface was scraped to achieve the initial target overlying clay layer height.

Experimental procedure

All foundation penetration tests were performed at a penetration velocity υ such that the dimensionless penetration rate V ($= \upsilon D/c_v$; where D is the foundation diameter and c_v is the coefficient of consolidation of the clay, which was taken as 2 m^2/yr) was 120 (the respective penetration velocity for each test is given in Table 2). This ensured undrained penetration through the clay layers and drained penetration in the sand layer (Lee *et al*., 2013a). In all cases the foundation was penetrated into the sample until it was within one diameter of the base of the centrifuge strongbox or channel. To minimise the influence of disturbances caused by prior tests the smaller foundations were tested first in the drum centrifuge channel followed by the larger foundations. Fifteen tests spaced at a minimum of 3D centre-to-centre were performed in the drum centrifuge channel while two tests were performed on opposing sides of each strongbox with a minimum spacing of ~2.7D (centre-to-centre). The potential boundary effects (bottom and sidewall) were assessed to be negligible at the final penetration depth using expressions and design charts derived from a database of large deformation numerical analyses reported in Ullah *et al*. (2014) and Ullah *et al.* (2016b). The penetration force was measured during the penetration using a load cell at the top of the shaft of the foundation.

During the visualising experiments high-resolution images of the exposed plane of the model were captured using the system described by Stanier & White (2013). In brief, the camera used was a 5 megapixel Prosilica GC2450C machine vision camera coupled with a Goya C-Mount 8 mm focal length lens. Illumination of the model was provided by two large LED panels located above and below the field of view (FOV). Diffusing lenses were used to minimise glare in the images captured. Images were captured and downloaded, in-flight, in real-time using a Gigabit Ethernet link passed across a fibre-optic rotary joint at a rate of 5Hz throughout the penetration tests. The image capture times were synchronised with the actuator position, enabling direct correlation of the image and foundation position.

At the end of testing, the half foundation models used in the visualising experiments were placed against the transparent window and penetrated into water to calibrate for buoyancy and potential window friction. Similar buoyancy calibrations were also performed for the full drum channel non-visualising experiments.

Model geometries

The geometry of each layered model is described throughout as ratio of the layer heights (H_{ct} and H_s) to the foundation diameter (D) (Figure 2 a). A wide range of H_{ct}/D = 0-1.07 and H_s/D = 0.25-1.04 ratios was modelled, covering the range of practical interest (punch-through has not been reported for $H_s/D>1$ (Hu *et al*., 2014a)). The spudcan and flat foundation geometries are illustrated in Figures 2 b and 2 c and the sizes summarised in Table 1. The spudcan had a shallow base inclination of 13^{o} with a 76^{o} protruding spigot, resembling the Marathon LeTourneau design class (SDC 82) widely used to support jack-up structures offshore. The flat foundations used in the non-visualising experiments performed in the drum centrifuge channel had a radiused underside matching the distance from the centre of rotation of the drum centrifuge to the clay surface. This improved the initial contact of the flat foundations with the sample on touchdown (Lee *et al*., 2013a).

To maximise the range of normalised geometries and facilitate cross comparisons, the drum centrifuge channel was divided into three sections (sections a, b and c). Section a had the maximum sand height. Following completion of the tests planned within Section a, the upper clay was removed allowing the sand layer to be scraped further to achieve a thinner sand layer before a layer of clay was consolidated atop. This process was repeated for Sections b and c to model a wide range of normalised geometries.

Soil properties

The soil properties for each experiment are listed in Table 2, using the notation shown on Figure 2 a. The relative density (I_D) and effective unit weight of the sand (γ'_s) were estimated using the maximum and minimum void ratios (e_{max} and e_{min}) reported by Lee *et al*. (2013a) for superfine silica sand in two different ways. For the visualising experiments performed in strongboxes the sand pluviation apparatus was carefully calibrated to create samples of a specific relative density. For the non-visualising experiments performed in the drum channel, 38 mm diameter tube samples were extracted allowing the relative density to be measured volumetrically. There is the potential that this manual sampling process caused some minor sample disturbance, however, it was chosen not to use alternative methods such as CPT correlations as the sand layer heights in these models were deemed too small to generate reliable measurements using a miniature CPT (Lunne et al. 1997). The average relative densities of the sand layers were 74% in the visualising experiments and 51% in the non-visualising experiments respectively. The constant volume friction angle (φ_{cv}) of the superfine sand was taken as 31º (after Lee *et al*., 2013a).

Following the foundation penetration tests, epoxy ball penetrometer tests (Lee *et al*., 2012) were conducted in the underlying clay layer after carefully removing the top clay and sand layers to minimise disturbance due to possible down-drag of sand and clay beneath the penetrometer. An intermediate roughness ball factor of N_{ball} = 13.5 was used to measure the in-situ undrained shear strength profile of the clay. These measurements were adjusted to account for the OCR (due to removal of the sand and clay layers, which was done to preclude entrapment of material beneath the penetrometer) using the following equation after Ladd *et al*. (1977):

$$\frac{s_u}{\sigma'_{vo}} = aOCR^b \qquad (1)$$

where, s_u is the undrained shear strength of clay in kPa, σ'_{vo} is the present effective vertical stress in kPa and a and b are fitting parameters that are back-fitted. From these measurements the in-situ undrained shear strength at the mudline (s_{um}), the top (clay-sand) and bottom (sand-clay) layer intercepts (s_{uti} and s_{ubi}) and the gradients of strength with depth (ρ_{ct} and ρ_{cb}) were inferred. The effective unit weight of the clay layers (γ'_{ct} and γ'_{cb}) were measured by oven drying 20 mm diameter samples extracted from each of the layers.

LOAD PENETRATION RESPONSES DURING PUNCH-THROUGH

Visualising experiments: clay interbedded with dense sand (I_D = 74%)

Figure 3 shows the twelve load-penetration curves measured during the visualising drum centrifuge experiments. The responses are grouped in Figure 3 a and c and Figure 3 b and d to isolate the effect of H_{ct} and H_s for the spudcan and flat foundations respectively. In all the analyses the load reference plane is taken at the maximum base area ($A = \pi D^2/4$) of the spudcan and the nominal bearing resistance q_{nom} is defined as the net vertical load ($F_{net} = F_{total} - F_{buoyancy} - F_{friction}$; where $F_{buoyancy}$ and $F_{friction}$ were derived by the aforementioned calibration process) divided by the maximum spudcan area ($q_{nom} = F_{net}/A$). Many of the load penetration responses show a region of reducing penetration resistance indicative of a punch-through response. For the majority of the curves the q_{nom} values are within the range (192-960 kPa) typical for jack-up operations (Young *et al.*, 1984).

For spudcans, the bearing pressure does not increase significantly until the underside of the spudcan is fully in contact with the mudline (full embedment), whereas for flat foundations the rise in resistance is immediate. The resistance increases linearly with depth because the undrained shear strength of the top clay layer increases approximately linearly with depth and the bearing factor reaches a constant value at a very shallow embedment in soft clay. Eventually the influence of the interbedded sand layer causes the resistance to rise more rapidly as the sand layer is mobilised. This is referred to as the transitional depth d_t because the mechanism is transitioning from a classical spudcan bearing capacity mechanism (soil flowing laterally and upwards around the spudcan) to a punch-through peak resistance type mechanism (with a block of soil beneath the spudcan being punched downwards). When this punch-through mechanism is mobilised the peak resistance q_{peak} occurs. As the foundation punches through the sand layer into the underlying clay, the resistance initially reduces before rising once more when the spudcan is fully penetrated into the underlying clay. In this region the resistance rises because the undrained shear strength of the underlying clay layer increases with depth. The severity of the reduction in penetration resistance post-q_{peak} and the depth over which $q_{nom} < q_{peak}$ determine the severity of a punch-through type failure.

Figure 4 a and Figure 4 b illustrate that q_{peak} increases with both H_{ct}/D and H_s/D. For a spudcan and intermediate normalised sand height ($H_s/D = 0.67$), increasing H_{ct}/D over the range of 0 (i.e. sand-clay) to 0.91, q_{peak} rises by ~ 63% (see Figure 4 a). For H_{ct}/D of ~ 0.65, increasing H_s/D over the range of 0.33-1 increases q_{peak} by ~ 250% (see Figure 4 b). Thus, H_s/D has a more significant impact on q_{peak} than H_{ct}/D for this particular series of experiments. Similar trends are evident with respect to d_{punch} as illustrated in Figure 4 c and Figure 4 d: H_s/D has a dominant effect on the magnitude of d_{punch} compared to H_{ct}/D.

Non-visualising experiments: clay interbedded with medium dense sand (I_D = 51%)

Figure 5 shows the fifteen load-penetration curves measured during the non-visualising drum centrifuge tests (12 spudcan and 3 flat foundations) performed in three different sections of the drum centrifuge channel to yield a range of normalised geometries. The general characteristics of response in clay-sand-clay are the same as described in the previous section for the visualising experiments: H_s/D dominates H_{ct}/D with respect to the magnitude of q_{peak} and d_{punch}. However, due to the lower relative density (I_D = 51%) of the sand layer the q_{peak} values are generally smaller than those of I_D = 74% in Figure 3. Aside from this difference, one other key observation can be made from this set of data: smaller D typically leads to greater q_{peak} and more severe punch-through, whereas larger D tends to result in a plunging type failure (Hu *et al.* 2013) where $q_{nom} \approx q_{peak}$ for several meters. The same trend was found by Lee *et al*. (2013a) for similar sand-clay experiments.

Figure 6 isolates the effect of H_{ct} for D of 16, 8 and 6 m for tests conducted in Sections b and c of the drum centrifuge channel where H_s was 4 m. By increasing H_{ct} by 2.32 m (in prototype terms), q_{peak} increased by 7, 10 and 19 % for D =16, 8 and 6 m respectively. Hence, the effect of H_{ct} on q_{peak} is more significant for smaller D (i.e. greater H_{ct}/D).

Figure 7 isolates the effect of H_s for D of 16, 12 and 6 m for tests conducted in Sections a and b of the drum centrifuge channel where H_{ct} was ~ 6 m. By increasing H_s by 2.25 m (in prototype terms), q_{peak} increased by 15, 30 and 30 % for D =16, 12 and 6 m respectively. Hence, the effect of H_s on q_{peak} is also more significant for smaller D (i.e. greater H_s/D).

FAILURE MECHANISMS DURING PUNCH-THROUGH

This section presents the results of PIV analyses performed on the digital images captured during the visualising tests performed in a strongbox within the drum centrifuge channel. Incremental vectorial displacements are plotted over a displacement increment of ~ 0.06 m (prototype scale) using an amplification factor of 20 for clarity. All analyses were conducted using the GeoPIV software (White *et al*. 2003). The subset size adopted was 50 $\times$ 50 pixels and the spacing was 10 pixels. The vertical and horizontal displacement contours are normalised by the foundation displacement and plotted over the range of 0.1-1, at increments of 0.1. A normalised incremental displacement of unity indicates that the surrounding material moves at the same velocity as the foundation. In all cases, the top of the sand layer was taken as the vertical datum and the foundation size D was 6 m for consistency with Figure 3 where the depths and penetration resistances of each analysis is indicated.

Effect of H_{ct} on failure mechanisms in the top clay layer

The failure mechanisms for a spudcan (test T1SP) and flat foundation (test T1FL) in a thin top clay layer are shown at a penetration of ~ 0.5 m from the mudline in Figure 8. When the top layer of clay is thin – as shown in Figure 8 – the soil immediately squeezes radially because the comparatively strong layer of sand beneath it confines the failure mechanism to the upper clay layer. This is similar to the squeezing behaviour explored by Meyerhof & Chaplin (1953) except that some vertical component of soil movement is also noted. However, the occurrence of this effect is dependent upon the top clay layer height. When the top clay layer is thick – as shown in Figure 9 – the mechanisms resemble those typical of shallow foundations; in particular, the cavity expansion model of McMahon *et al*. (2013).

The expected squeezing mechanism in clay as identified in Figure 8 is not evident in the thick top clay layer when the foundations approach the sand layer. Figure 10 shows the failure mechanisms when the foundations are in close proximity to the sand layer and it is clear that the radial squeezing is minimal. This observation is similar to that derived via similar PIV tests performed with a larger foundation (D = 12 m) penetrating soft over stiff clay (Hossain *et. al.* 2011). These findings contradict the current industry guidelines (ISO, 2012; SNAME, 2008) where radial soil squeezing is assumed for soft over stiff stratigraphies irrespective of the soft layer height. Possible reasons for the deviation from the squeezing theory include: (i) that the theory of Meyerhof & Chaplin (1953) is based on soft over rigid stratum (i.e. Young's modulus, E = ∞), whereas here although the interbedded sand is comparatively strong, the stiffness is finite; and (ii) as a consequence of (i) the sand layer deforms vertically, thus discouraging radial squeezing.

Peak failure mechanisms

The failure mechanisms at q_{peak} are shown in Figure 11. An inverted truncated cone of clay and sand is shown to be pushed into the bottom clay layer. Both the clay and sand appear to shear along the periphery of the inverted truncated cone of soil, as indicated by the displacement magnitudes in the vector plot (Figure 11 a and d) and the closeness of the vertical displacement contours (Figure 11 b and e). In the underlying clay layer, the displacements appear broadly similar to those that occurred in the thick clay layer (Figure 9), indicating that the bearing capacity generated by the clay layer could potentially be approximated using simple shallow foundation bearing capacity expressions following Lee *et al*., (2013b). Some load spreading is evident because the width mobilised at the surface of the bottom clay layer is larger than the foundation diameter, though the inclination of this load spreading is of the order of a few degrees and significantly less than the ~11-18 degrees recommended in the projected area method in the current industry guidelines (SNAME, 2008; ISO, 2012). A partial back flow of clay above the foundation is also apparent, which leads to a reduction in capacity as it causes an increase in the vertical loading. The failure mechanism at q_{peak} is not significantly different for the flat foundation compared to the spudcan.

The digital images captured during these experiments were further interrogated to derive general geometries of the soil failure mechanisms for foundation peak resistances (Figure 13 a). The images showed that a thin band of clay (of height H_c) was entrapped beneath the foundation and sheared during mobilisation of the peak resistance. Measurement of the entrapped clay layer geometry using close-range photogrammetry (see Figure 12 b) yielded the following linear relationship between the entrapped clay layer height H_c and the in-situ top clay layer height H_{ct}:

$$H_c = 0.07 H_{ct} \qquad 2$$

This means, on average, 7% of the top clay layer height was entrapped beneath the foundation (for both flat and spudcan foundations tested here). For the limiting case where H_{ct} is zero (i.e. sand - clay), H_c is zero.

Similarly, the effective sand height (H_{eff}) during shearing was measured from the images and is compared with the previous reported measurements in sand-clay experiments in Figure 12 c. The following relation, identified originally by Teh *et al.* (2008), appears to be equally valid for clay-sand-clay stratigraphies:

$$H_{eff} = 0.88 H_s \qquad 3$$

The depth of mobilisation of peak resistance d_{peak}, can be estimated from the schematic in Figure 12 a as follows:

$$d_{peak} = H_{ct} + 0.12H_s - H_c \quad (4)$$

As the entrapped plug thickness (H_c plus H_s) increases, d_{peak} reduces (i.e. the peak resistance is mobilised earlier during the penetration). By combining Equations 2 and 4, d_{peak} can be expressed as a function of the in-situ layer heights as follows:

$$d_{peak} = 0.93H_{ct} + 0.12H_s \quad (5)$$

The measured and predicted d_{peak} from Equation 5 show reasonable agreement with the majority of the predictions falling within 25% bounds (see Figure 12 d). The good agreements between the predictions and measurements in Figure 12 c and d provide the potential scope for the two layer (sand-clay) model of Hu *et al*. (2014) to be extended to three layer (clay-sand-clay) geometries.

Bearing capacity mechanism in the underlying clay

Figure 13 shows that a plug of soil is entrapped beneath the foundation during penetration into the underlying clay layer. The plug is composed of a thin layer of clay and thicker layer of sand, the thicknesses of which can be predicted using Equations 2 and 3. In the spudcan foundation tests, the view from the transparent window showed that the size of the entrapped plug was reducing with further penetration into the underlying clay layer. Initially this was thought to be due to the conical underside of the foundation encouraging the soil within the plug to flow around the footing, since the reduction in the sand plug size was not observed in the flat foundation tests. However, comparing the bearing capacity factor N_c (= q_{nom}/s_u) after penetration of 0.5D and 1D into the bottom clay layer for spudcan and flat foundations for all layer geometries, the bearing capacity factors were found to be almost identical irrespective of whether the soil plug size appeared to diminish in the images. This makes it unlikely that the entrapped plug was reducing in volume during penetration. Instead, it is possible that the conical underside of the spudcan encourages the sand in the plug to flow away from the transparent window of the strongbox. This is further confirmed by the post-dissected full spudcan sample data in clay-sand-clay presented in Hossain (2014), where a sand plug depth of 0.85-0.9H_s was consistently measured.

Figure 13 shows the deeply embedded bearing capacity mechanism for one of the flat foundation tests (T3FL). The majority of the plug is moving vertically downward with the foundation and a small triangular wedge is also formed beneath the plug. The closeness of the vertical contours indicates that the clay surrounding the plug periphery is shearing. Overall the mechanism looks very similar to that identified for sand-clay stratigraphies by Teh *et al*. (2008), except that a thin layer of clay is entrapped immediately beneath the foundation. Values for N_c were back-calculated from the q_{nom} measurements as follows:

$$N_c = \frac{\left(q_{nom} - \gamma'_{cb} H_{fdn}\right)}{s_u} \qquad 6$$

where s_u is the undrained shear strength at the base of the foundation (i.e. at the load reference plane) and H_{fdn} is defined using the schematic in Figure 12 a as:

$$H_{fdn} = 0.88H_s + 0.07H_{ct} + t \qquad 7$$

where t is the foundation thickness. The N_c values varied in the range of ~13-24 with greater entrapped plug volumes leading to higher N_c values. These values are much higher than those measured and simulated using large deformation finite element analyses reported by Hossain *et al.* (2009) for spudcan penetration in a single clay layer, where N_c was shown to be ~12-13. Such large N_c values are a direct result of the large soil plug entrapment under the foundation where the height of the composite foundation can be estimated using Equation 7 above. The increased height of the composite foundation provides additional shear resistance around the entrapped plug periphery and mobilises deeper soil with a higher strength than the s_u value used in the definition of N_c at the foundation base level (Craig and Chua, 1990) resulting in higher N_c values than for penetration into a single layer of clay. For sand over clay soil, large N_c values over a similar range as observed here were obtained by Lee *et al*. (2013a) through centrifuge testing and by Hu *et al*. (2014a) through large deformation finite element analyses. For a comprehensive assessment of the performance of the equations derived here (Equations 5-7) see the companion paper of Ullah *et al.* (2016a).

PERFORMANCE OF CURRENT INDUSTRY APPROACHES FOR PREDICTING PUNCH THROUGH

The peak bearing capacity (q_{peak}) determines the amount of preload that can be safely applied to the foundation without inducing punch-through failure. Accurate q_{peak} prediction is therefore extremely important. In addition, prior to installing a jack-up foundation, a complete punch-through risk assessment typically involves determining the potential depth of the punch-through event, d_{punch}.

The existing industry guidelines (SNAME, 2008; ISO, 2012) recommend the projected area (PA) (also known as load-spread) and punching shear (PS) methods. In the PA approach, upper and lower bound projection angles (α_p) corresponding to 18.43° (1h:3v where, h: horizontal, v: vertical) and 11.31° (1h:5v) are recommended in both guidelines. In the PS approach, the SNAME (2008) and ISO (2012) guidelines differ in their recommendations of choosing a suitable punching shear coefficient K_s. SNAME (2008) recommends choosing a lower bound K_s where the sand frictional properties are ignored and replaced with clay strength properties as follows:

$$K_s \tan\varphi' = \frac{N s_{ubi}}{\gamma'_s D} \qquad 8$$

Where φ' is the peak operative friction angle, γ'_s is the sand effective unit weight and s_{ubi} is the bottom sand-clay intercept strength. A lower bound value of N = 3 is recommended. Alternatively ISO (2012) provides a single design chart for estimation of K_s after Hanna & Meyerhof (1980) for friction angles (φ') of 25°-40° at 5° intervals. Interpolation or extrapolation is required for intermediate values. The typical range for Ks is between ~0.5-12. There is no clear recommendation for choosing the operative friction angle when estimating K_s. A constant volume friction angle ($\varphi' = \varphi_{cv}$) was assumed in these predictions.

As noted by Hu *et al*. (2015) there is some ambiguity in the ISO (2012) guidelines regarding the position of the surcharge in the calculations. To comprehensively explore the performance of the existing industry guidelines, calculations were performed by both considering and ignoring the effective weight of the sand frustum (W_{SF}) when calculating the surcharge term. In the PA method, when neglecting the effect of the weight of the sand plug (hollow markers) the expression used was:

$$q_{peak} = \left[\left(s_c N_c s_{ubi} + q_o\right)\left(1 + 2\frac{H_s}{D}\tan\alpha_p\right)^2 \right] \qquad 9$$

Whereas when accounting for the weight of the sand plug (filled markers) the expression used was:

$$q_{peak} = \left[\left(s_c N_c s_{ubi} + q_o\right)\left(1 + 2\frac{H_s}{D}\tan\alpha_p\right)^2 \right] - \left[\left(1 + 2\frac{H_s}{D}\tan\alpha_p\right)^2 \gamma'_s H_s \right] \qquad 10$$

Similarly, in the PS method, when neglecting the effect of the weight of the sand plug (hollow markers) the expression used was:

$$q_{peak} = \left(s_c N_c s_{ubi} + q_o\right) + \left[2\frac{H_s}{D}\left(\gamma'_s H_s + 2q_o\right) s_s K_s \tan\varphi'\right] \tag{11}$$

Whereas when accounting for the weight of the sand plug (filled markers) the expression used was:

$$q_{peak} = \left(s_c N_c s_{ubi} + q_o\right) + \left[2\frac{H_s}{D}\left(\gamma'_s H_s + 2q_o\right) s_s K_s \tan\varphi'\right] - \gamma'_s H_s \tag{12}$$

Here, s_s represents the shape factor and is assumed as 1. Both PA and PS methods recommended in the guidelines are for two-layer stiff over soft soil conditions. The effect of the top soft clay (H_{ct}) was accounted for in the predictions in this paper by assuming that the top clay layer acts as a further surcharge:

$$q_o = H_{ct}\gamma'_{ct} \tag{13}$$

where γ'_{ct} is the effective unit weight of the top clay.

The performance of these two methods and both interpretations (accounting for and neglecting the self-weight of the sand plug) are shown in Figure 14. In addition to the experimental data reported in this paper, three tests on clay-sand-clay (I_D = 89%) reported by Hossain (2014) have been added. Both PA and PS approaches underestimate q_{peak}. In all cases neglecting the effective sand frustum weight provides a minor improvement in the q_{peak} estimation, leading to small improvements in the statistical parameters the ratio of measured to calculated q_{peak} (mean, standard deviation (SD) and coefficient of variation (COV)). The predictions can only be forced to converge with the measurements by either: (i) adopting very high values of α_p for the PA method, thus implying extremely high load-spread angles (i.e. higher than the ~11°-18° range recommended in industry guidelines) that would contradict the PIV observations in Figure 11; or (ii) adopting very high values for the punching shear coefficient K_s. There is no rational basis for either modification.

The conservative predictions generated by the PA and PS approaches are similar to those found for the two layer of sand-clay case (Hu *et al.*, 2015). For the two-layer sand-clay case, such conservatism principally occurs because neither method accounts for the stress-level dependent response of the sand shearing at mobilisation of q_{peak} (as seen here in Figure 12 for the three-layer clay-sand-clay case). This indicates that development of a stress-level dependent approach for predicting q_{peak} – like that described by Hu *et al*. (2014a) for the sand-clay case – would likely lead to improvements in the predictions for the clay-sand-clay cases presented here.

Estimation of d_{punch} requires accurate estimation of both q_{peak} and the bearing capacity factor (N_c) for the bottom clay layer at a depth where $q_{nom} = q_{peak}$ (see Figure 3 a). For the SNAME (2008) and ISO (2012) methods, N_c is recommended to be calculated after Houlsby and Martin (2003). The equivalent cone angle β was 180° and 154° for flat and spudcan foundations respectively with the surface roughness α taken as 0.2 following Hossain *et al*. (2005) as the foundations had a smooth finish.

Figure 15 shows the measured N_c plotted versus the predicted N_c at d_{punch} indicating that the N_c values predicted using Houlsby & Martin (2003) are extremely conservative because the presence of the entrapped sand plug observed in Figure 13 is unaccounted for.

The impact that this consistent conservatism has on the d_{punch} predictions in Figure 16 is fortuitous: under-predictions for q_{peak} and N_c result in generally acceptable predictions of d_{punch} for all methods. One example of the beneficial effect of these compensating errors is highlighted in Figures 14-16 (test T3SP; see also Figure 3) for the ISO (2012) PS approach (blue marker): although q_{peak} and N_c are underestimated by ~ 40% (Figure 14) and by ~ 58% (Figure 15) respectively, d_{punch} is predicted very well due to the compensating errors and falls on the line of equality (Figure 16). Additionally, the under predictions of q_{peak} lead to a number of cases where punch-through was not predicted, even though punch-through of several meters occurred (at prototype scale) was observed in the experiments. Alternative expressions for predicting q_{peak} and N_c that explicitly account for stress-level dependent sand response and the presence of the entrapped plug are required to generate reliable assements for the risk of punch-through for clay-sand-clay stratgraphies. To improve on the industry guidelines, the authors' have developed an extension of the analytical model of Hu *et al*. (2014a) based on the observed PIV failure mechanisms that has been reported in the companion paper (see Ullah *et al.*, 2016a).

CONCLUSIONS

Centrifuge tests modelling foundation punch-through on clay-sand-clay stratigraphies of varying geometry have been reported for both conical spudcan and flat based foundation shapes. Two series of experiments were described (visualising strongbox and non-visualising full drum channel tests) resulting in a database of twenty-seven load-displacement curves for clay interbedded with both medium dense and dense sand. Punch-through was observed for a wide range of stratigraphy geometries. Digital images recorded during the visualising experiments were analysed using PIV techniques to identify the soil flow mechanisms at key stages during punch-through. The peak resistance q_{peak}, bearing capacity factor N_c where $q_{nom} = q_{peak}$ and the depth of punch-through d_{punch} were predicted using current industry guidelines and compared to measurements from the experiments. This led to the following conclusions:

- q_{peak} is dependent on both the normalised top clay height (H_{ct}/D) and sand height (H_s/D). For constant H_{ct}/D, increasing H_s/D results in a significant increase in q_{peak}. For constant H_s/D, increasing H_{ct}/D also results in a moderate increase in q_{peak}.

- The failure mechanism in the top clay layer was controlled by H_{ct}/D in the experiments presented in this paper, with progressively lower H_{ct}/D values promoting more radial squeezing of soil. Due to differences in mechanisms the soft over stiff soil squeezing theories recommended by ISO (2012) and SNAME (2008) are not generally applicable in modelling the rapid increase in resistance above the sand layer. Alternative methods of predicting the resistance in the top clay layer are required.

- During mobilisation of q_{peak} a thin band of top clay becomes entrapped beneath the foundation and shears at the periphery of the foundation along with sand beneath. A load spreading type mechanism occurs where the load is projected onto a larger bearing area on the bottom clay than the foundation area. Simple expressions were derived from measurements of the geometries at q_{peak} using the digital images. The heights of the entrapped clay layer (H_c), effective sand layer height (H_{eff}) and the depth of the peak resistance (d_{peak}) were all shown to depend on the intact layer heights.

- A composite soil plug comprising of entrapped layers of clay and sand was shown to be pushed down into the bottom clay layer following punch-through. This generated additional shearing resistance because clay around the periphery of the entrapped plug sheared during further penetration. This results in a significant increase in bearing capacity factor N_c compared to either the Houlsby & Martin (2003) relation recommended by SNAME (2008) and ISO (2012) or those derived for a spudcan on single layer clay by Hossain & Randolph (2009).

- The current industrial guidelines provided by SNAME (2008) and ISO (2012) are overly conservative in predicting q_{peak} and N_c where $q_{nom} = q_{peak}$. The compensating errors fortuitously result in generally acceptable prediction of the punch-through depth d_{punch}. However, many cases where punch-through occurred in the experiments were predicted to not be at risk of punch-through. Alternative expressions for predicting q_{peak} and N_c – that explicitlty account for stress-level dependent sand response and the presence of the entrapped plug – are required to generate reliable assesments for the risk of punch-through for clay-sand-clay stratgraphies.

- The experiments reported provides a database for developing and verifying an extension of the stress-level dependent punch-through models for sand-clay stratigraphies (Lee *et al*., 2013b; Hu *et al*., 2014a) to account for the presence of the overlying clay layer in clay-sand-clay stratigraphies.

ACKNOWLEDGEMENTS

The research presented here forms part of the activities of the Centre for Offshore Foundation Systems (COFS), currently supported as a node of the Australian Research Council Centre of Excellence for Geotechnical Science and Engineering (grant CE110001009) and through the Fugro Chair in Geotechnics, the Lloyd's Register Foundation Chair and Centre of Excellence in Offshore Foundations and the Shell EMI Chair in Offshore Engineering (held by the fourth author). The authors would like to acknowledge the additional support from the Australian Research Council (ARC) through Discovery Project No. 1096764. Thanks are due to the UWA drum centrifuge technicians Bart Thompson and Greg Outridge.

REFERENCES

Baglioni, V. P., Chow, G. S. & Endley, S. N. (1982). Jack-Up rig foundation stability in stratified soil profiles. In *Proceedings of Offshore Technology Conference*, OTC 4409, pp. 363-384.

Bienen, B. & Cassidy, M. J. (2013). Set up and resulting punch-through risk of jack-up spudcans during installation. *Journal of Geotechnical and Geoenvironmental Engineering* **139(12)**:2048-2059.

Bienen, B., Ragni, R., Cassidy, M. J. & Stanier, S. A. (2015). Effects of consolidation under a penetrating footing in carbonate silty clay. *Journal of Geotechnical and Geoenvironmental Engineering* **04015040**.

Craig, W. H. & Chua, K. (1990). Deep penetration of spudcan foundations on sand and clay. *Géotechnique* **40**(4), 541-556.

Dier, A., Carroll, B. & Abolfathi, S. (2004). Guidelines for jack-up rigs with particular reference to foundation integrity. Health and Safety Executive (HSE), Research report 289, UK, pp. 1-91.

Dutt, R. N. & Ingram, W. B. (1984). Jackup rig siting in calcareous soils. In *Proceedings of*. Offshore Technology Conference, OTC 4840, pp. 541-548.

Hanna, A. M. & Meyerhof, G. G. (1980). Design charts for ultimate bearing capacity of foundations on sand overlying soft clay. *Canadian Geotechnical Journal* **17(2)**:300-303.

Hossain, M. S. (2014). Experimental investigation of spudcan penetration in multi-layer clays with interbedded sand layers. *Géotechnique* **64(4)**:258-276.

Hossain, M. S., Hu, Y., Randolph, M. F. & White, D. J. (2005). Limiting cavity depth for spudcan foundations penetrating clay. *Géotechnique* **55(9)**:679-690.

Hossain, M. S. & Randolph, M. F. (2009). New mechanism based design approach for spudcan foundations on single layer clay. *Journal of geotechnical and geoenvironmental engineering,ASCE* **135(9),** 1264-1274.

Hossain, M. S., Randolph, M. F. & Saunier, Y. N. (2011). Spudcan deep penetration in multi-layered fine-grained soils. *International Journal of Physical Modelling in Geotechnics* **11(3):** 100-115.

Houlsby, G. T. & Martin, C. M. (2003). Undrained bearing capacity factors for conical footings on clay. *Géotechnique* **53(5)**:513-520.

Hu, P., Stanier, S. A., Cassidy, M. J. & Wang, D. (2014a). predicting peak resistance of spudcan penetrating sand overlying clay. *Journal of Geotechnical and Geoenvironmental Engineering* **140(2)**:04013009

Hu, P., Wang, D., Cassidy, M. J. & Stanier, S. A. (2014b). Predicting the resistance profile of a spudcan penetrating sand overlying clay. Can. Geotech. J. **51 (10)**, 1151-1164.

Hu, P., Stanier, S. A., Wang, D. & Cassidy, M. J. (2015). A comparison of full profile prediction methods for a spudcan penetrating sand overlying clay. *Géotechnique Letters* **5(3)**:131-139.

ISO (2012). ISO 19905-1: Petroleum and natural gas industries- site specific assessment of mobile offshore units-Part 1 : Jack-ups. Geneva, Switzerland : International Organization for Standardization.

Ladd, C. C., Foot, R., Ishihara, K., Poulos, H. G. & Schlosser, F. (1977). Stress-deformation and strength characteristics. In *Proc. 9th International Conference on Soil Mechanics and Foundation Engineering (ICSMFE)*.), vol. 2, pp. 421-494.

Lee, K. K., Cassidy, M. J. & Randolph, M. F. (2012). Use of epoxy in developing miniature ball penetrometers. *International Journal of Physical Modelling in Geotechnics* **12**:119-128.

Lee, K. K., Cassidy, M. J. & Randolph, M. F. (2013a). Bearing capacity on sand overlying clay soils: experimental and finite-element investigation of potential punch-through failure. *Géotechnique* **63(15)**:1271-1284.

Lee, K. K., Randolph, M. F. & Cassidy, M. J. (2013b). Bearing capacity on sand overlying clay soils: a simplified conceptual model. *Géotechnique* **63(15)**:1285-1297.

Lunne, T., Robertson, P. K. & Powell, J. M. (1997). Cone penetration testing in geotechnical practice. London, UK: Blackie Academic and Professional.

Mcmahon, B. T., Haigh, S. K. & Bolton, M. D. (2013). Optimal displacement mechanisms beneath shallow foundations on linear-elastic perfectly plastic soil. *Géotechnique* **63(16)**:1447-1450.

Meyerhof, G. G. & Chaplin , T. K. (1953). The compression and bearing capacity of cohesive layers. *British Journal of Applied Physics* **4(1)**:20-26.

SNAME (2008). Recommended Practice for Site Specific Assessment of Mobile Jack-Up Units. T & R Bulletin 5-5A 1st edn, rev 3. Alexandria, VA, USA : Society of Naval Architechts and Marine Engineers.

Stanier, S. A., Ragni, R., Bienen, B. & Cassidy, M. J. (2014). Observing the effects of sustained loading on spudcan footings in clay. *Géotechnique* **64(11)**:918-926.

Stanier, S. A. & White, D. J. (2013). Improved image-based deformation measurement in the centrifuge environment. *Geotechnical Testing Journal* **36(6)**:1-14.

Teh, K.L., Leung, C.F., Chow, Y.K. & Handidjaja, P. (2009). Prediction of punch-through for spudcan penetration in sand overlying clay. In *Proceedings of Offshore Technology Conference*, OTC 20060, pp. 1-14.

Teh, K. L., Cassidy, M. J., Leung, C. F., Chow, Y. K., Randolph, M. F. & Quah, C. K. (2008). Revealing the bearing capacity mechanisms of a penetrating spudcan through sand overlying clay. *Géotechnique* **58(10)**:793-804.

Teh, K. L., Leung, C. F., Chow, Y. K. & Cassidy, M. J. (2010). Centrifuge model study of spudcan penetration in sand overlying clay. *Géotechnique* **60(11)**:825-842.

Ullah, S.N., Hu,Y., Stanier, S. A. & White, D. J. (2014). LDFE study of bottom boundary effect in foundation model tests. *International Journal of Physical Modelling in Geotechnics* **14(3)**, 80-87

Ullah, S. N.,Stanier, S.A., Hu, Y. & White, D.J. (2016a). Foundation punch-through in clay with sand: analytical modelling. *Géotechnique (submitted).*

Ullah, S.N., Hu,Y., Stanier, S. A. & White, D. J. (2016b). Lateral boundary effects in centrifuge foundation tests. *International Journal of Physical Modelling in Geotechnics*, available online ahead of print.

Ullah, S.N. (2016). Jackup Foundation Punch-Through in Clay with Interbedded Sand. PhD thesis, University of Western Australia, Perth.

White, D. J., Take, W. A. & Bolton, M. D. (2003). Soil deformation measurement using particle image velocimetry (PIV) and photogrammetry. *Géotechnique* **53(7)**:619-631.

Young, A., Remmes, B. & Meyer, B. (1984). Foundation performance of offshore jack-up drilling rigs. *Journal of Geotechnical Engineering* **110(7)**:841-859.

LIST OF FIGURES

Figure 9: Soil displacements for a thin top clay layer at a penetration depth of ~0.5 m from the mudline for spudcan and flat foundations respectively (T1SP, T1FL): (a, d) vectorial displacements; (b, e) normalised vertical displacement contours; and (c, f) normalised horizontal displacement contours.

Figure 10: Soil displacements when in close proximity to the sand layer for spudcan and flat foundations respectively (T2SP, T2FL): (a, d) vectorial displacements; (b, e) normalised vertical displacement contours; and (c, f) normalised horizontal displacement contours.

Figure 11: Soil displacements at peak resistance for spudcan and flat foundations respectively (T3SP, T3FL): (a, d) vectorial displacements; (b, e) normalised vertical displacement contours; and (c, f) normalised horizontal displacement contours.

Figure 12: (a) Geometric definitions of effective sand height (H_{eff}) and height of entrapped clay (H_c); the observed relationship between (b) H_c and in-situ clay height H_{ct}; (c) H_{eff} and H_s; and (d) the measured and predicted peak resistance depths (d_{peak}).

Figure 13: Clay-sand plug entrapment during penetration into the underlying clay layer for a flat foundation test (T3FL).

Figure 14: Performance of current industrial guideline approaches in predicting q_{peak}: (a) projected area or load-spread method with spread ratio of 1h:3v; (b) projected area or load-spread method with spread ratio of 1h:5v; (c) SNAME (2008) punching shear approach; and (d) ISO (2012) punching shear approach.

Figure 15: Performance of current industrial guideline approaches in predicting N_c at q_{clay}=q_{peak}: (a) projected area or load-spread method with spread ratio of 1h:3v; (b) projected area or load-spread method with spread ratio of 1h:5v; (c) SNAME (2008) punching shear approach; and (d) ISO (2012) punching shear approach.

Figure 16: Performance of current industrial guideline approaches in predicting d_{punch}: (a) projected area or load-spread method with spread ratio of 1h:3v; (b) projected area or load-spread method with spread ratio of 1h:5v; (c) SNAME (2008) punching shear approach; and (d) ISO (2012) punching shear approach.

LIST OF TABLES

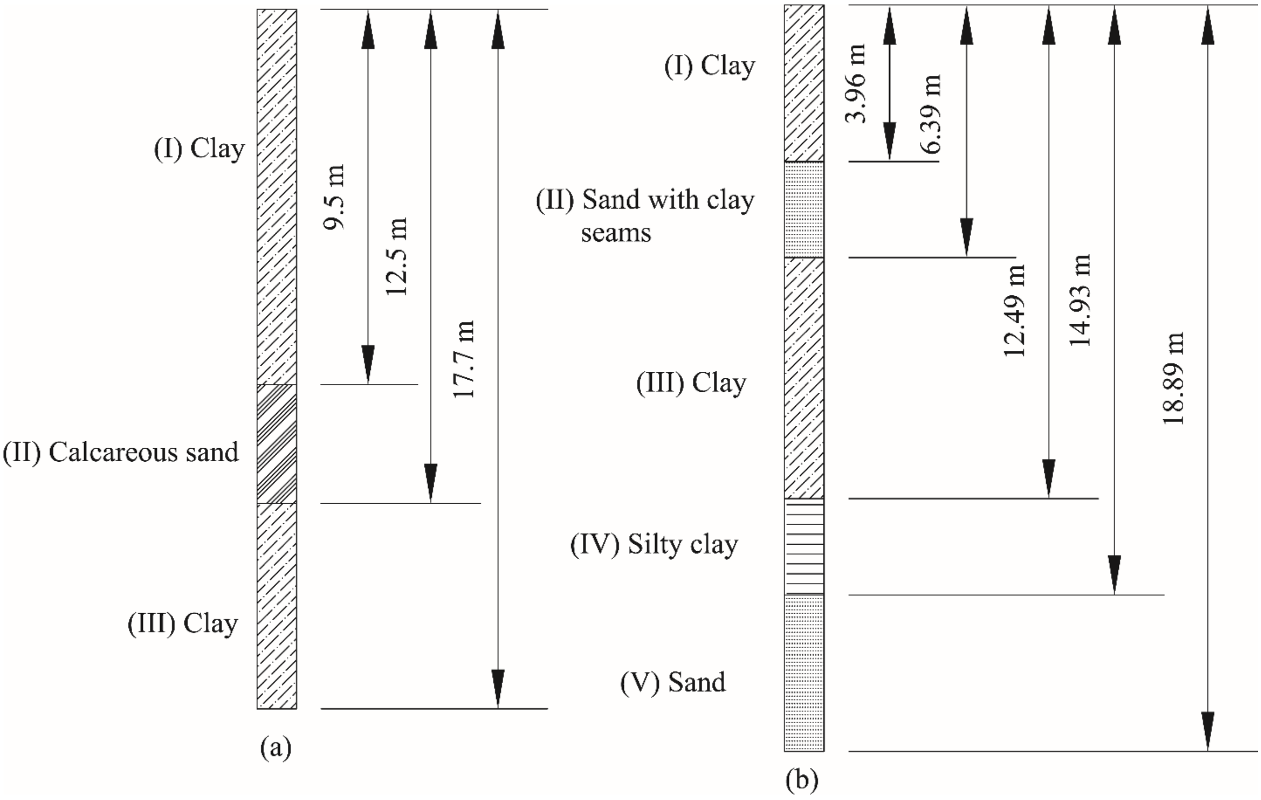

Figure 1: Example of clay-sand-clay stratigraphies: (a) Gulf of Suez (after Dutt & Ingram, 1984); and (b) Gulf of Mexico (after Baglioni *et al.* 1982).

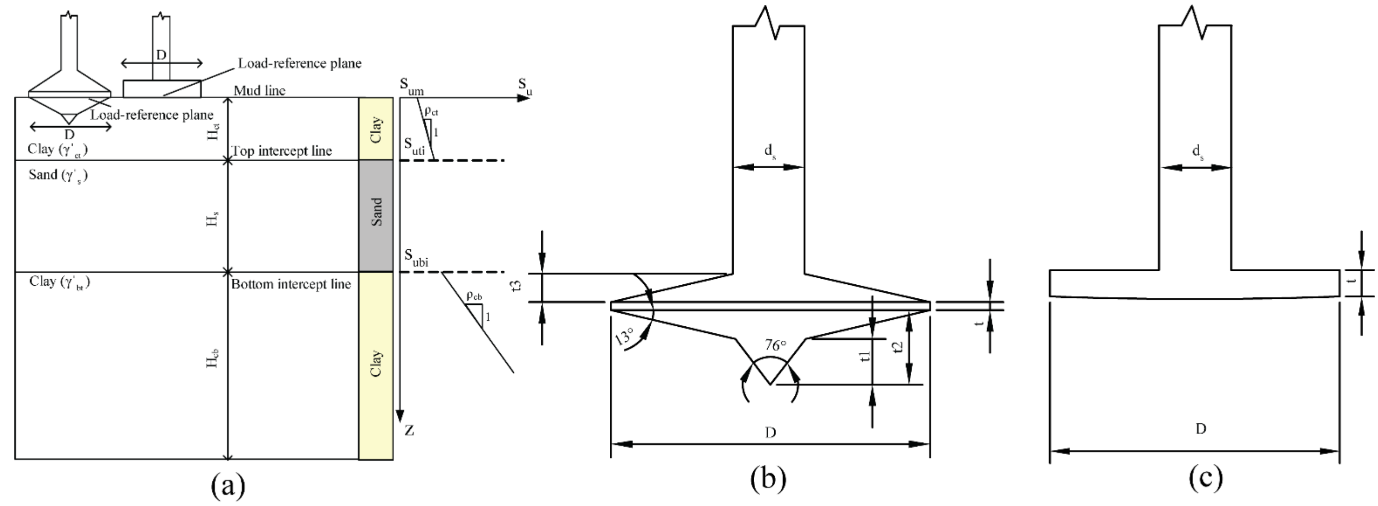

Figure 2: Soil layers and foundation geometries a) three layer clay-sand-clay stratigraphy, b) spudcan foundation and c) flat based foundation

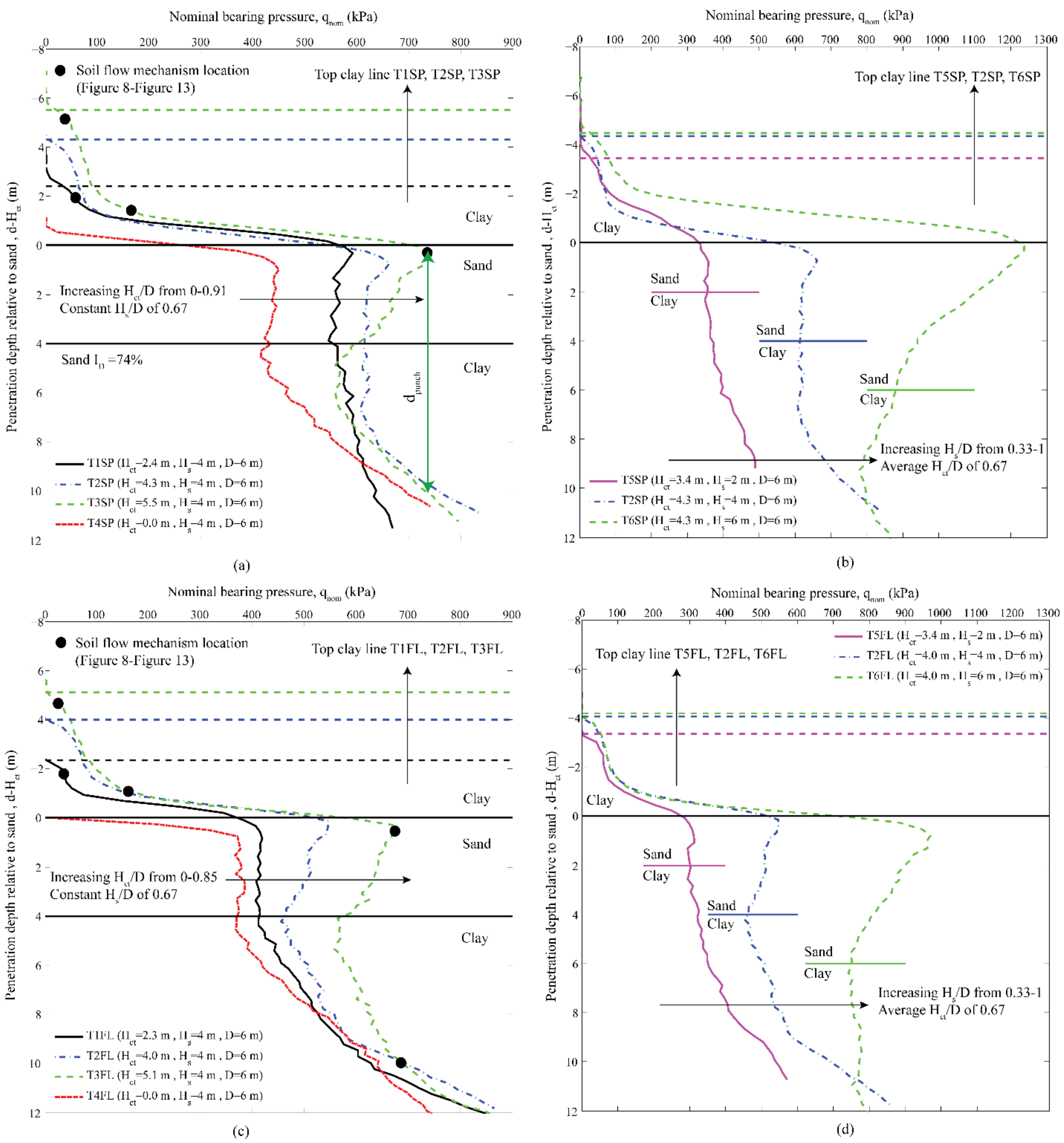

Figure 3: Load-penetration response of spudcan (a, b) and flat foundation (c, d) for clay with interbedded dense sand performed in drum centrifuge strongboxes (black dots represent soil flow mechanism locations reported in Figures 8-13).

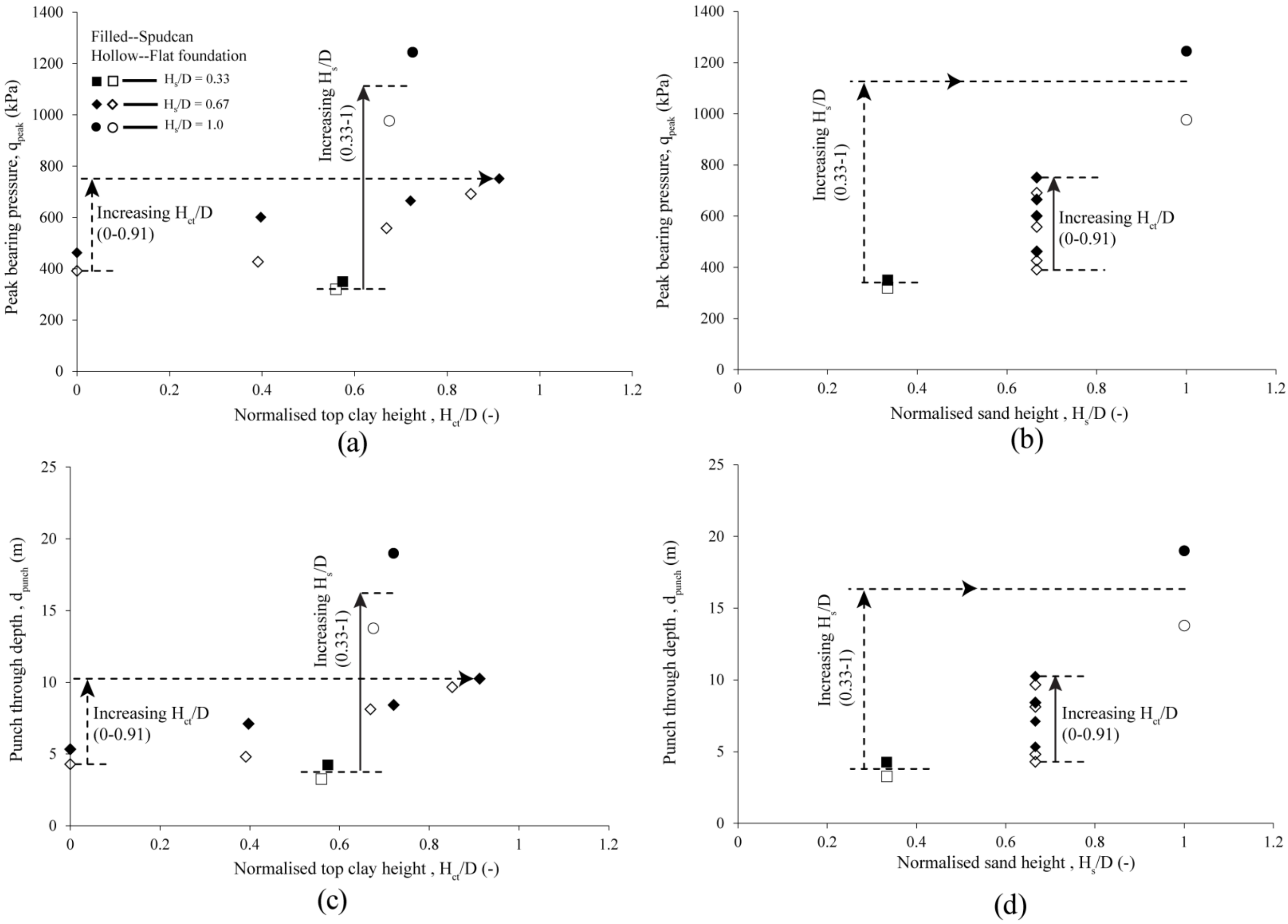

Figure 4: Effect of H_s/D and H_{ct}/D on q_{peak} and d_{punch}: (a) q_{peak} against normalised clay height H_{ct}/D; (b) q_{peak} against normalised sand height H_s/D; (c) d_{punch} against normalised clay height H_{ct}/D; and (d) d_{punch} against normalised sand height H_s/D.

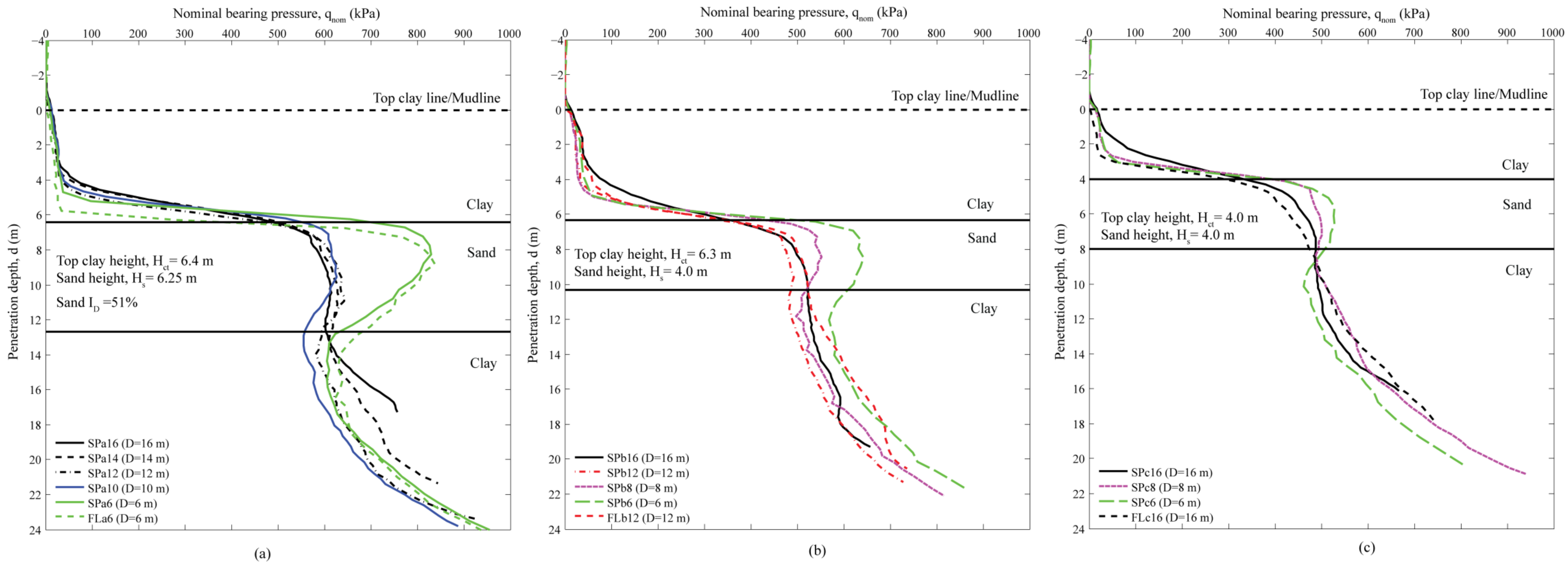

Figure 5: Load-penetration responses for spudcan and flat foundations in clay interbedded with medium dense sand performed in the drum centrifuge channel: (a) section a; (b) section b; and (c) section c.

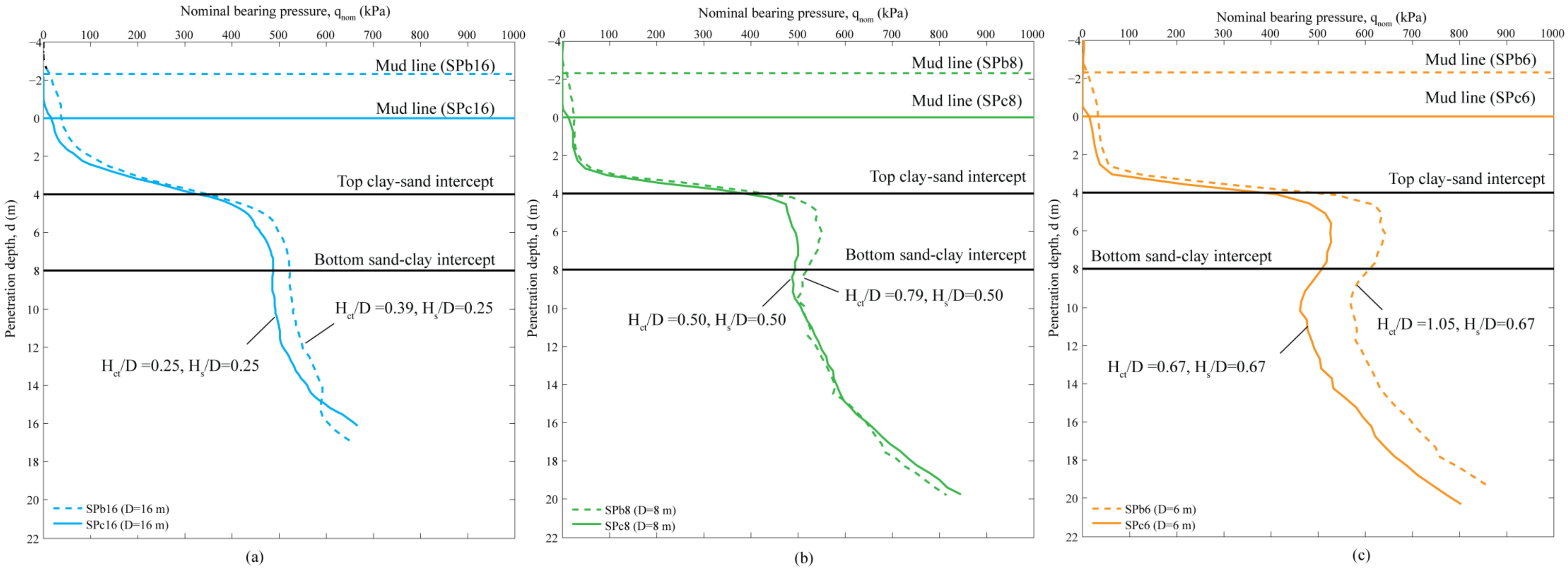

Figure 6: Effect of H_{ct}/D on the overall penetration resistance profile in medium dense sand (section b: H_{ct} = 6.32 m, H_s = 4 m and section c: H_{ct} = 4 m, H_s = 4 m).

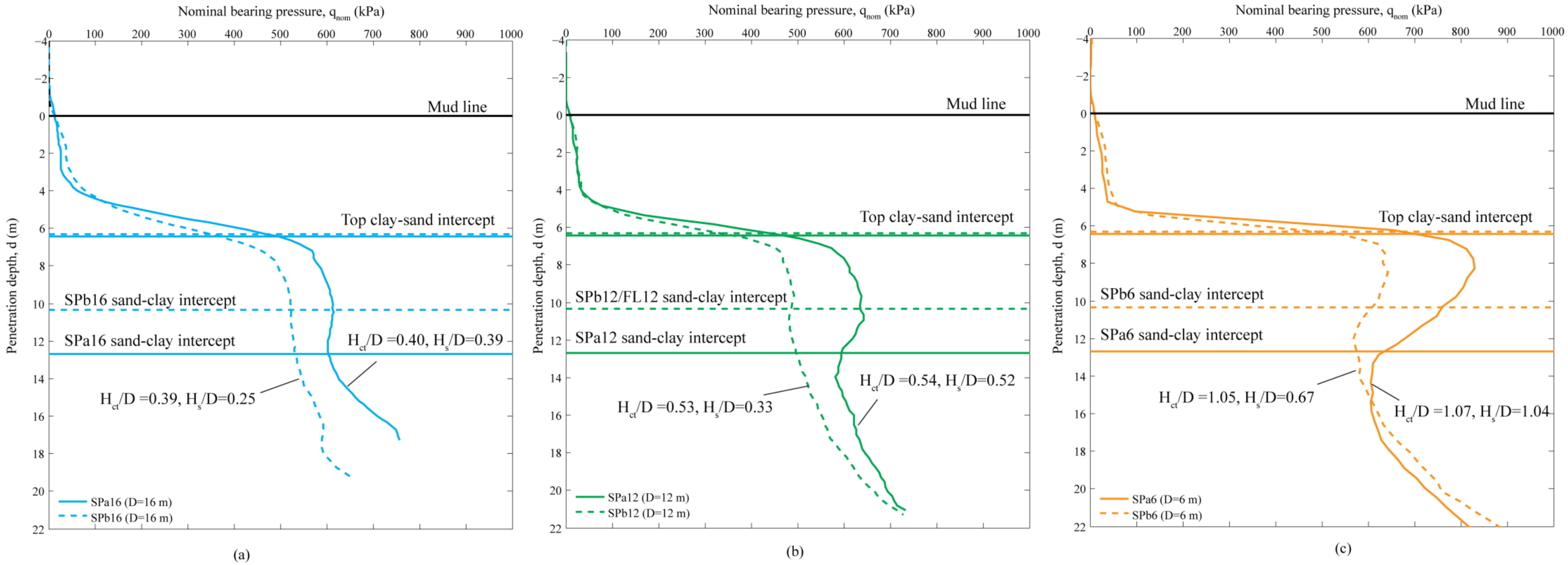

Figure 7: Effect of H_s/D on the overall penetration resistance profile in medium dense sand (section a: H_{ct} = 6.42 m, H_s = 6.25 m and section b: H_{ct} = 6.32 m, H_s = 4 m).

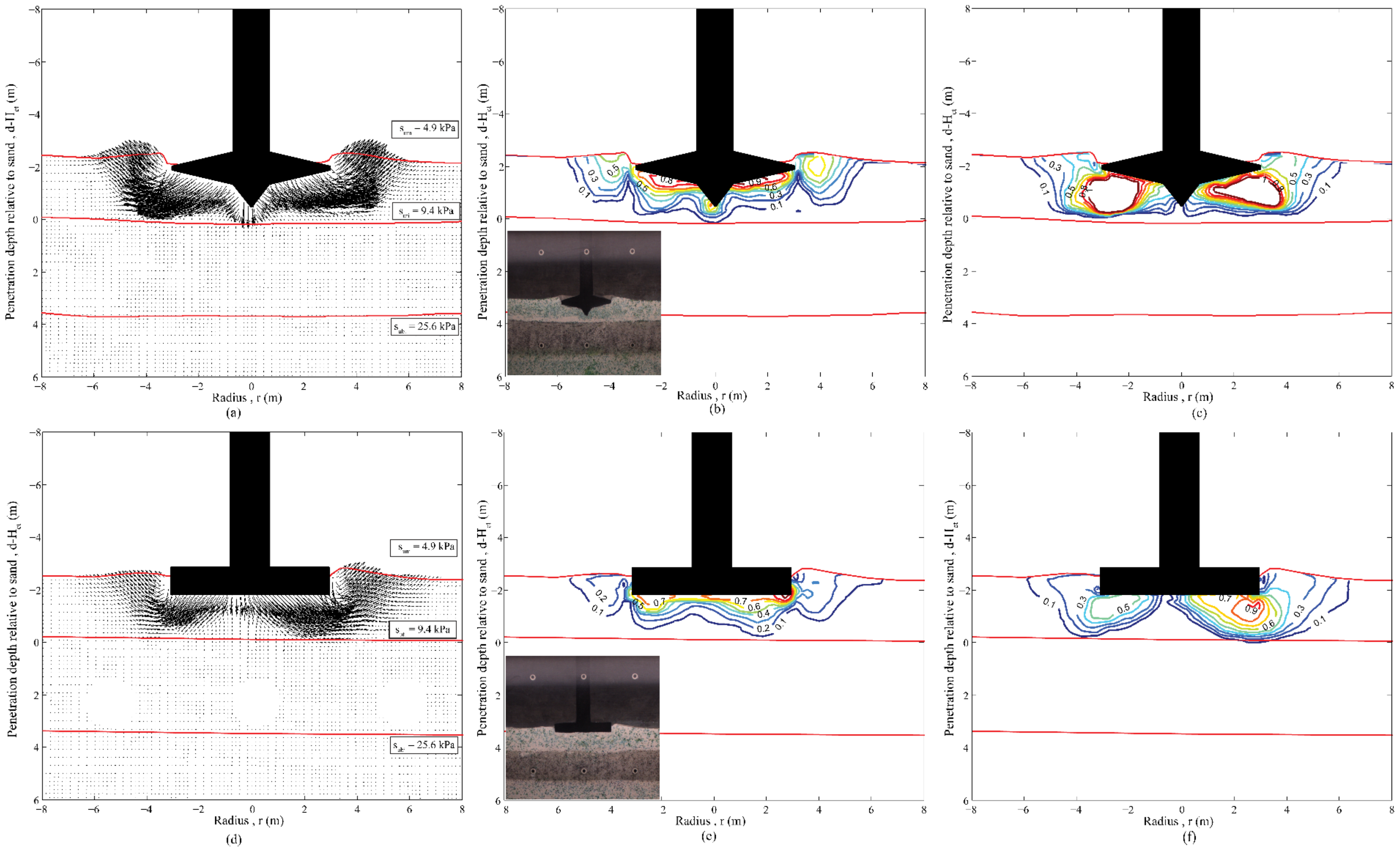

Figure 8: Soil displacements for a thin top clay layer at a penetration depth of ~0.5 m from the mudline for spudcan and flat foundations respectively (T1SP, T1FL): (a, d) vectorial displacements; (b, e) normalised vertical displacement contours; and (c, f) normalised horizontal displacement contours.

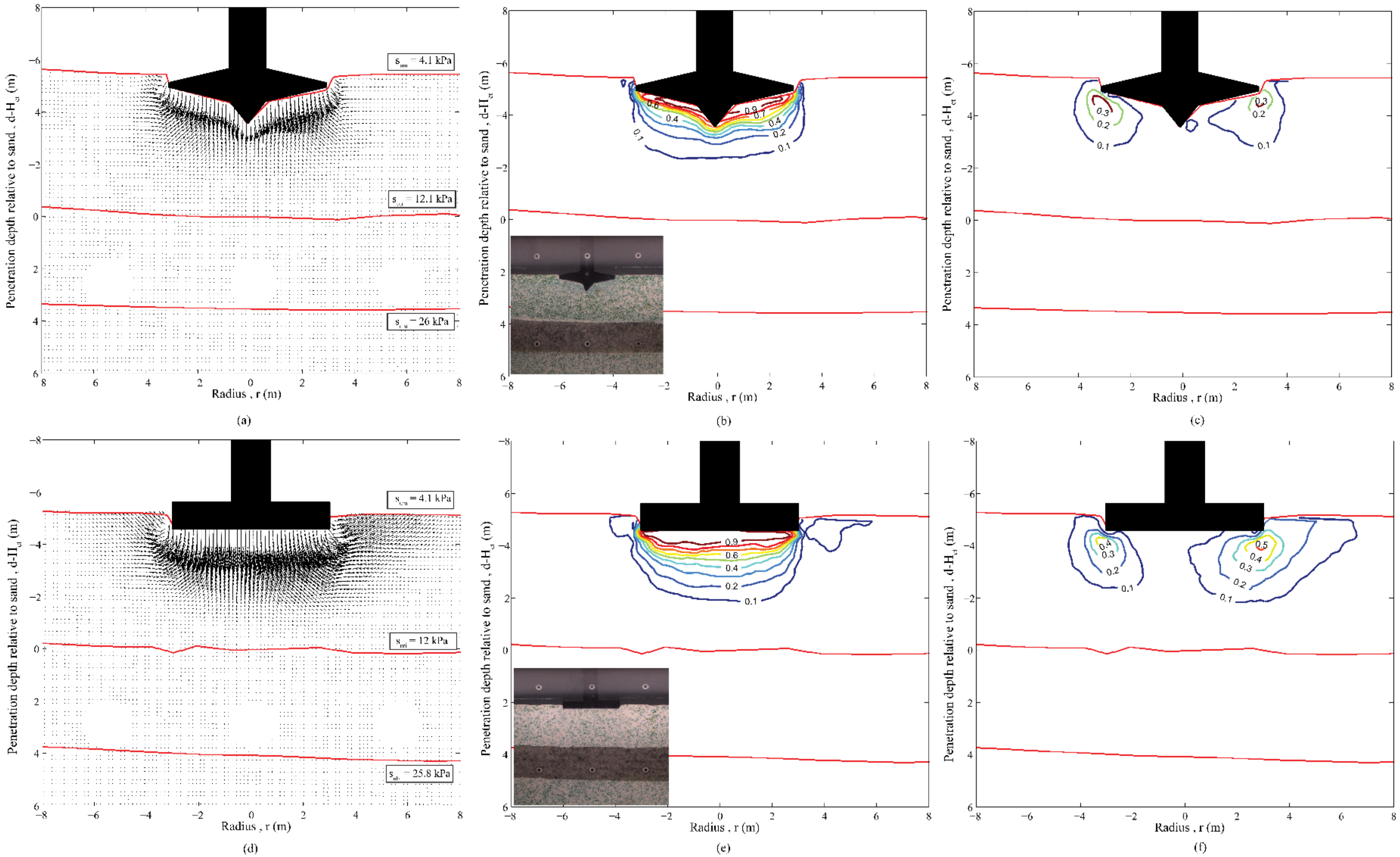

Figure 9: Soil displacements for a thick top clay layer at a penetration depth of ~0.5 m from the mudline for spudcan and flat foundations respectively (T3SP, T3FL): (a, d) vectorial displacements; (b, e) normalised vertical displacement contours; and (c, f) normalised horizontal displacement contours.

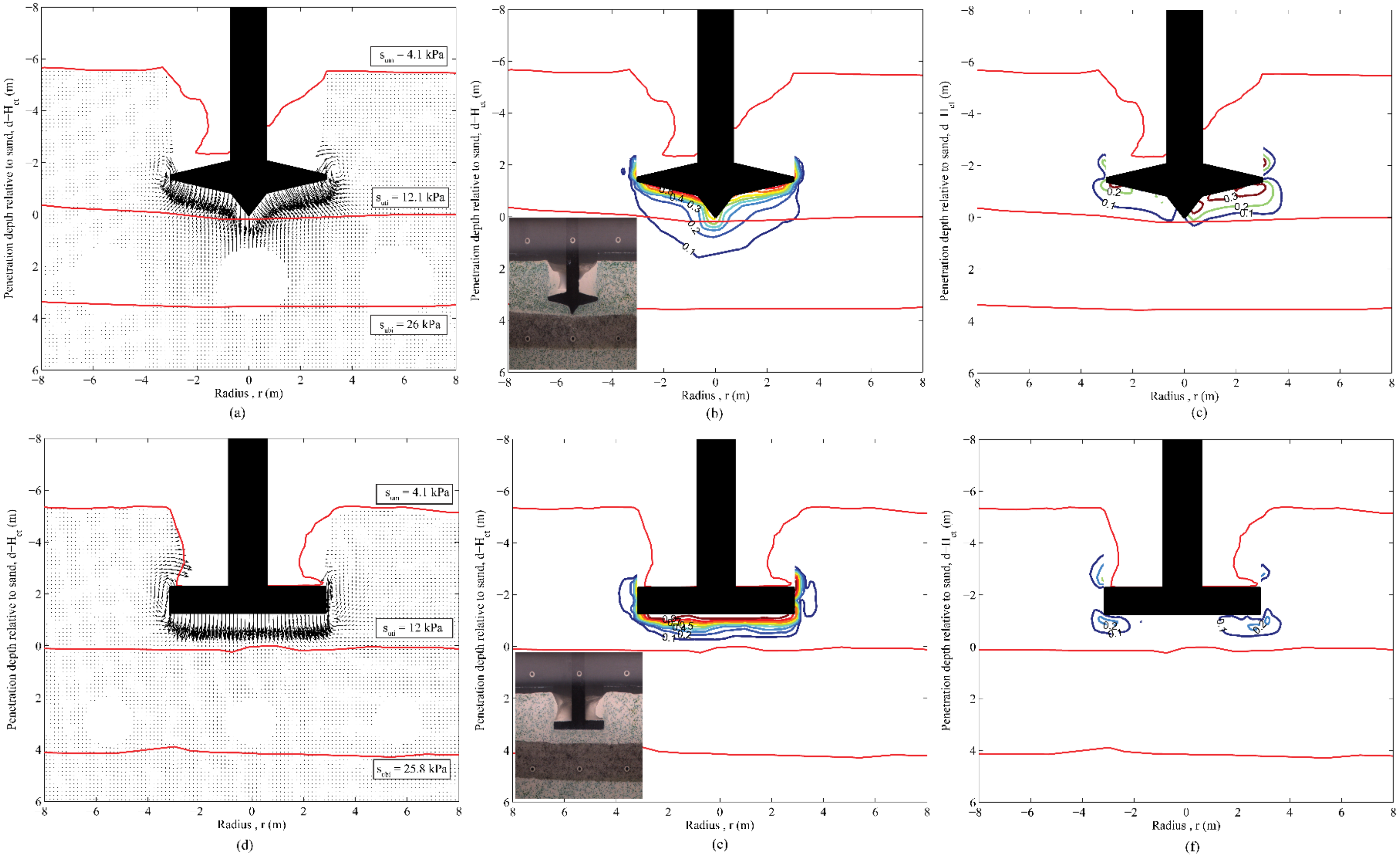

Figure 10: Soil displacements when in close proximity to the sand layer for spudcan and flat foundations respectively (T3SP, T3FL): (a, d) vectorial displacements; (b, e) normalised vertical displacement contours; and (c, f) normalised horizontal displacement contours.

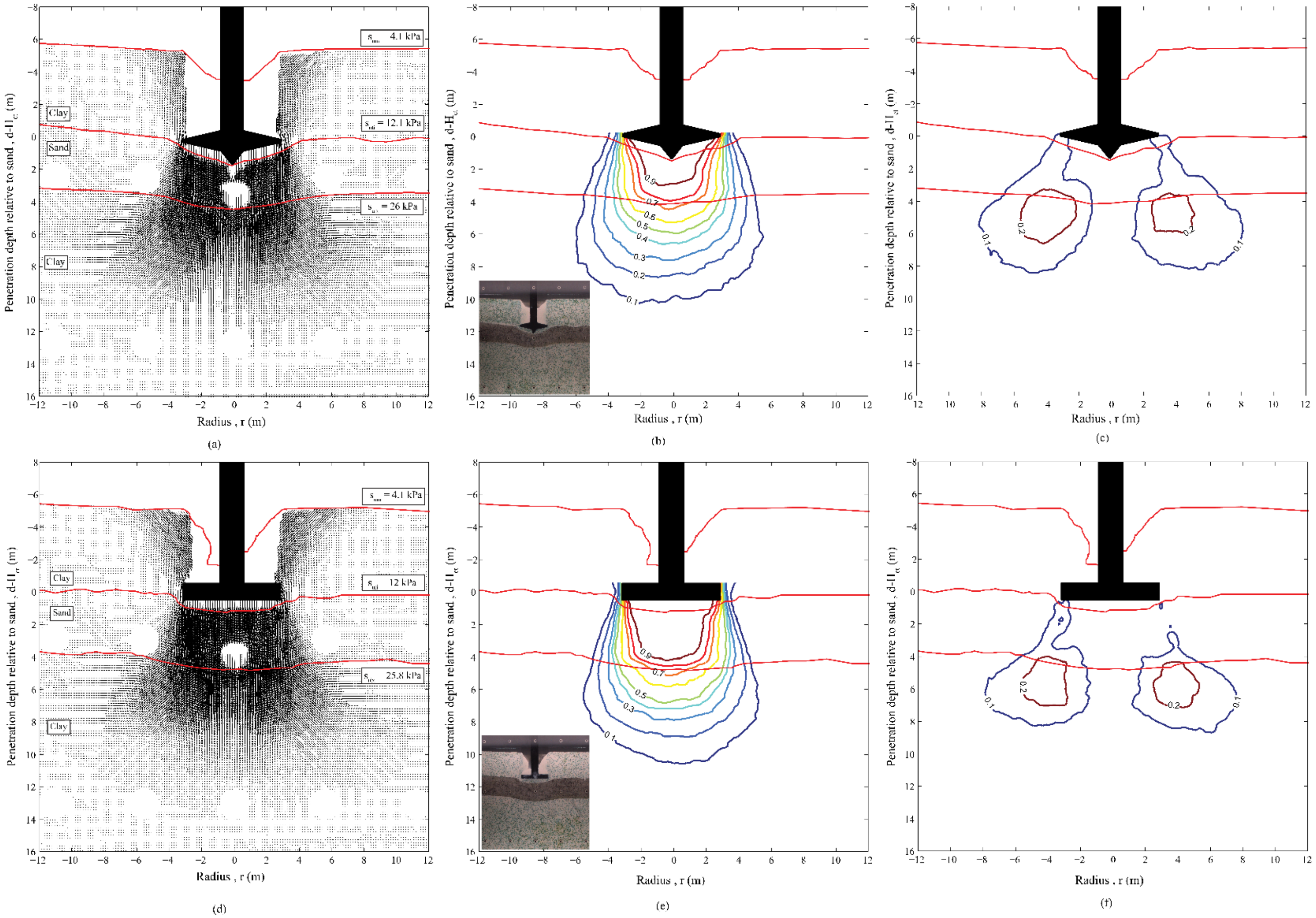

Figure 11: Soil displacements at peak resistance for spudcan and flat foundations respectively (T3SP, T3FL): (a, d) vectorial displacements; (b, e) normalised vertical displacement contours; and (c, f) normalised horizontal displacement contours.

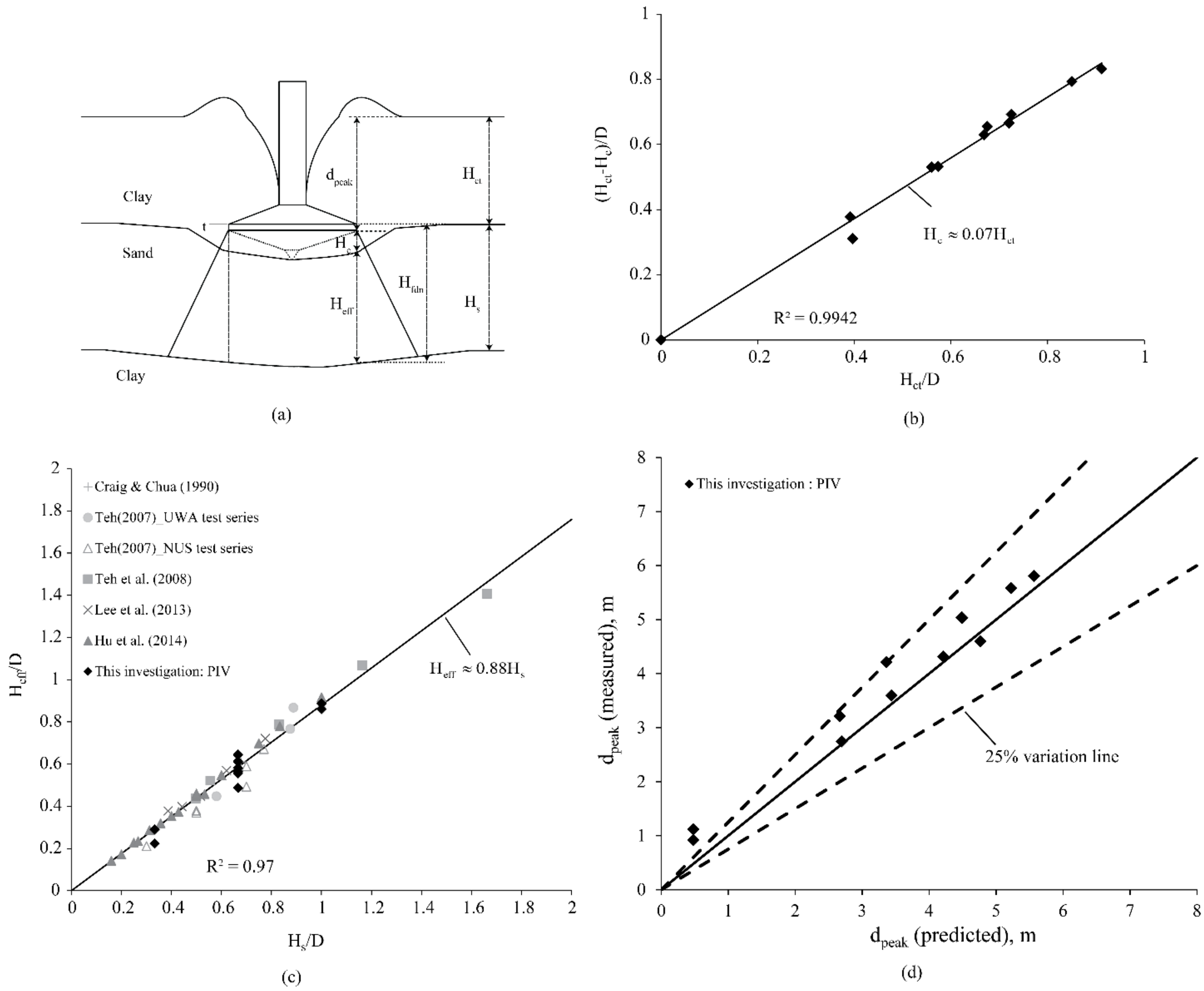

Figure 12: (a) Geometric definitions of effective sand height (H_{eff}) and height of entrapped clay (H_c); the observed relationship between (b) H_c and in-situ clay height H_{ct}; (c) H_{eff} and H_s; and (d) the measured and predicted peak resistance depths (d_{peak}).

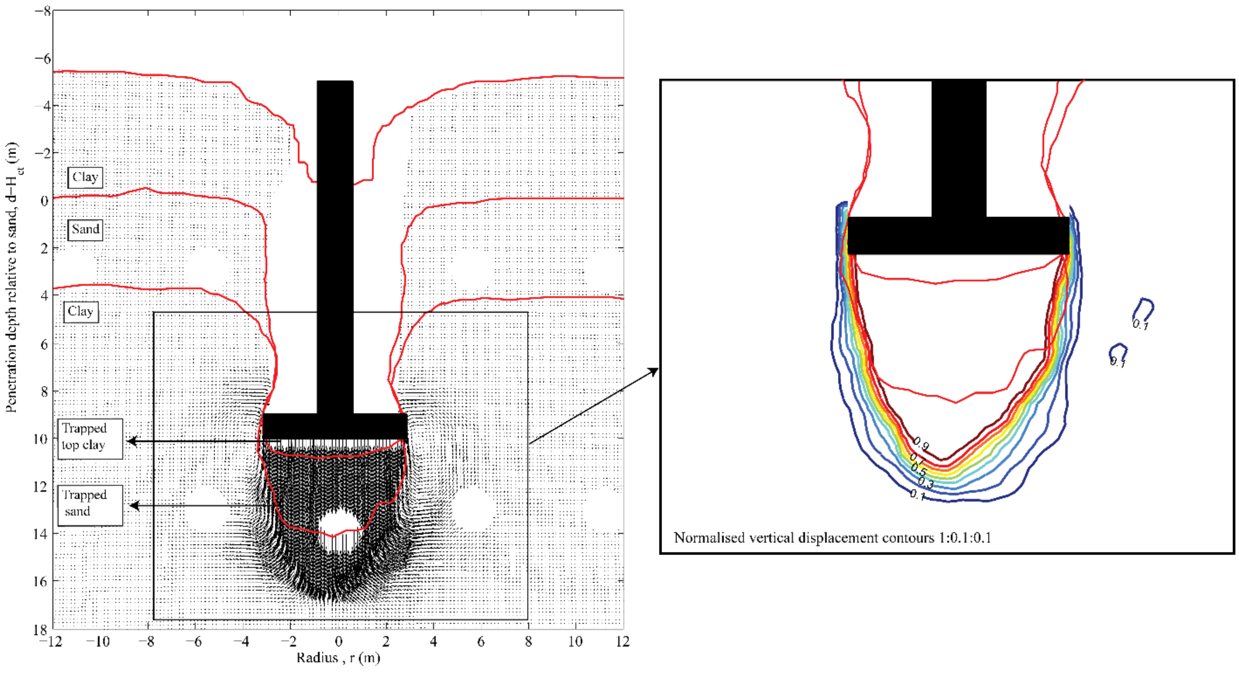

Figure 13: Clay-sand plug entrapment during penetration into the underlying clay layer for a flat foundation test (T3FL).

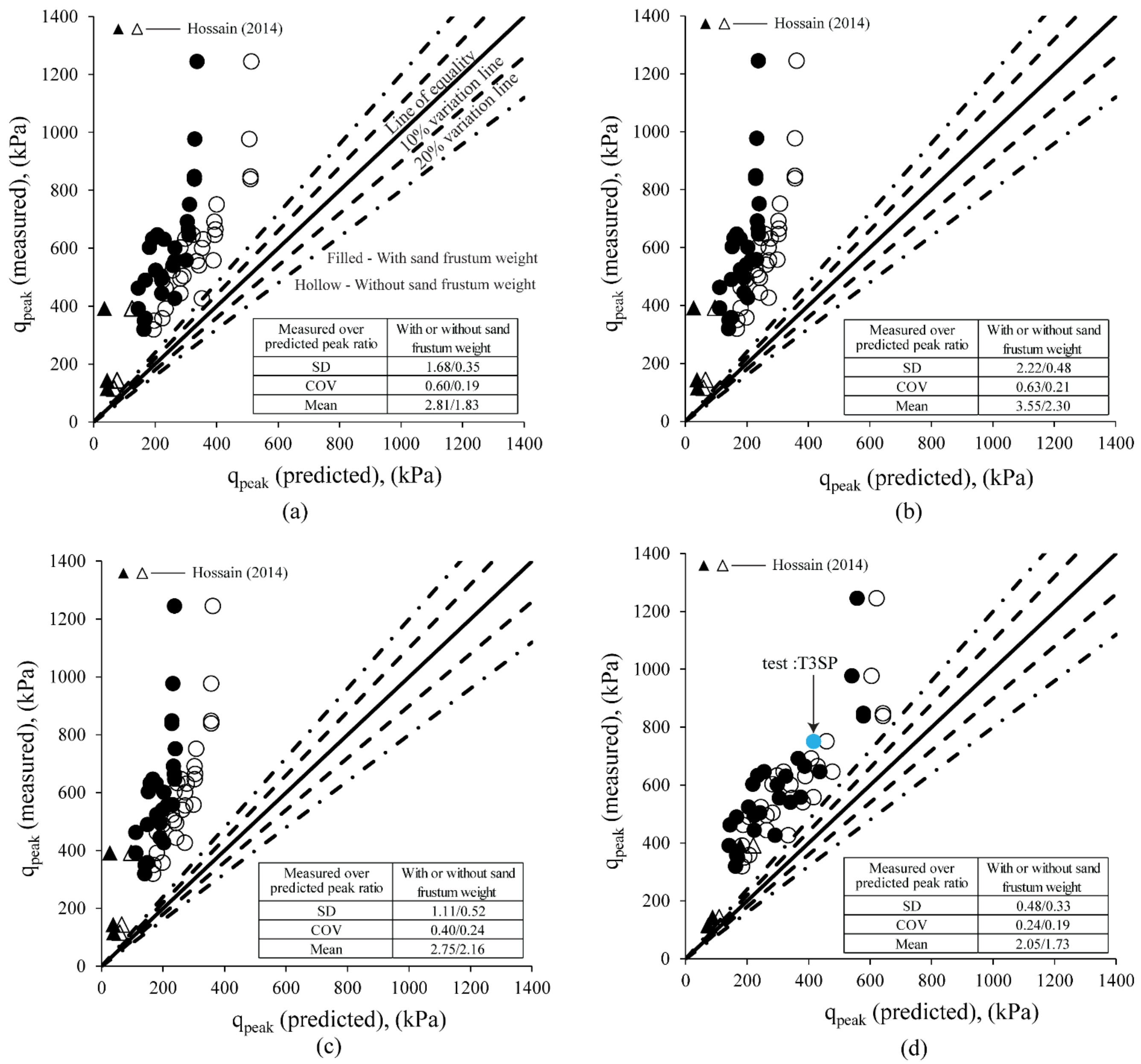

Figure 14: Performance of current industry guideline approaches in predicting q_{peak}: (a) projected area or load-spread method with spread ratio of 1h:3v (ISO and SNAME); (b) projected area or load-spread method with spread ratio of 1h:5v (ISO and SNAME); (c) SNAME (2008) punching shear approach; and (d) ISO (2012) punching shear approach.

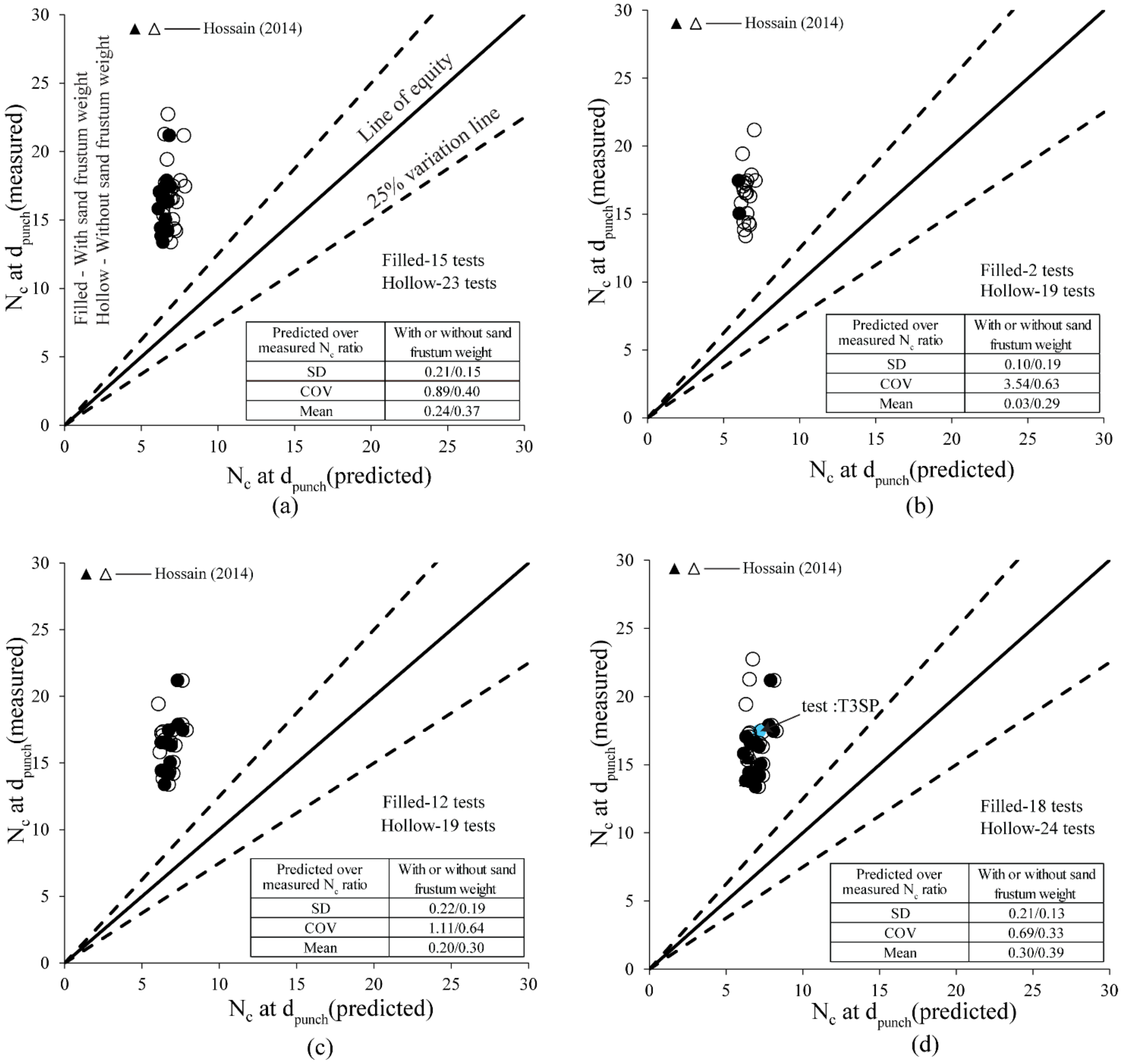

Figure 15: Performance of current industry guideline approaches in predicting N_c at $q_{clay}=q_{peak}$: (a) projected area or load-spread method with spread ratio of 1h:3v (ISO and SNAME); (b) projected area or load-spread method with spread ratio of 1h:5v (ISO and SNAME); (c) SNAME (2008) punching shear approach; and (d) ISO (2012) punching shear approach.

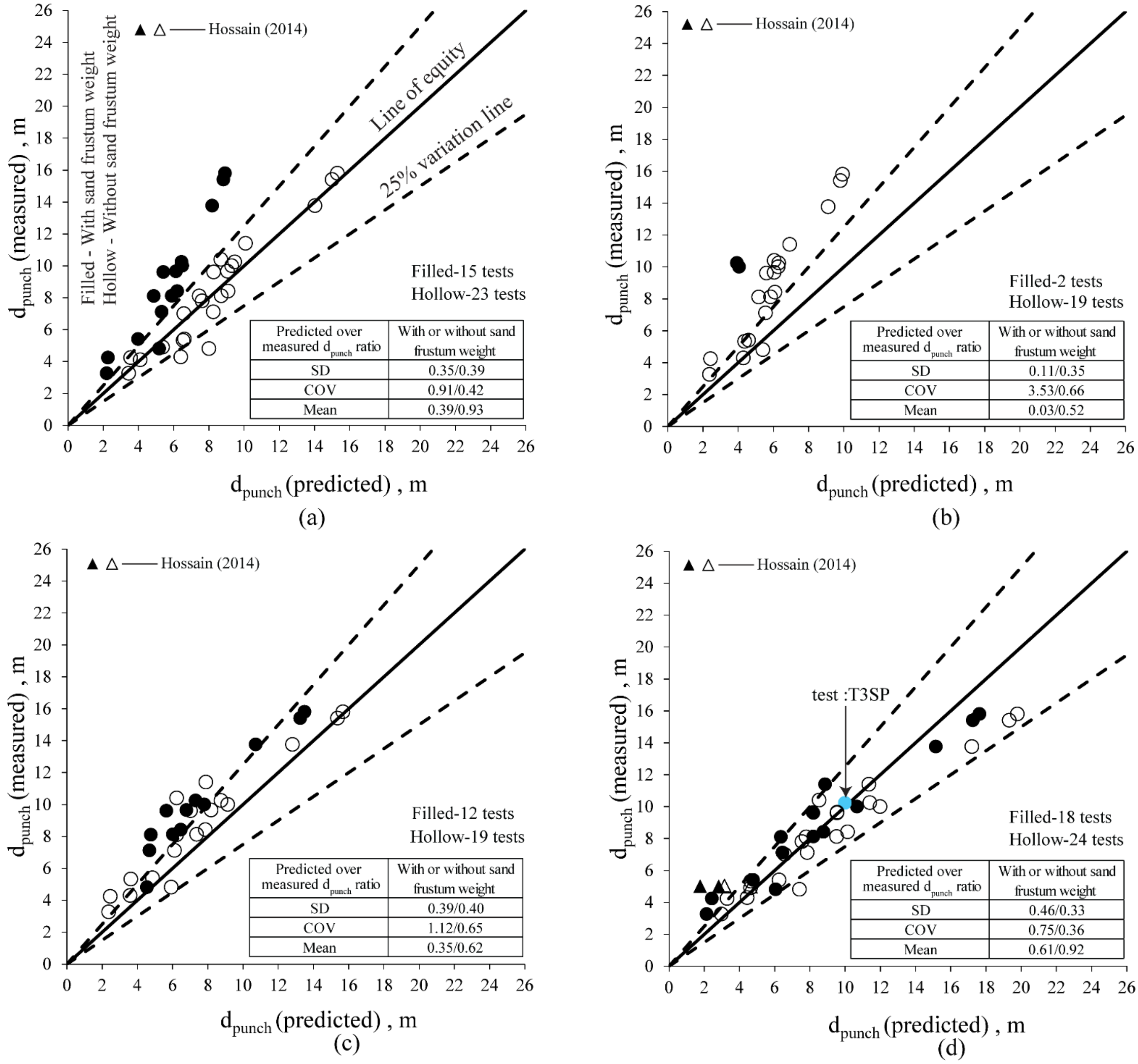

Figure 16: Performance of current industry guideline approaches in predicting d_{punch}: (a) projected area or load-spread method with spread ratio of 1h:3v (ISO and SNAME); (b) projected area or load-spread method with spread ratio of 1h:5v (ISO and SNAME); (c) SNAME (2008) punching shear approach; and (d) ISO (2012) punching shear approach.

Table 1: Foundation prototype geometries at 200g.

Type of foundation	D * (m)	d_s*(m)	t1* (m)	t2* (m)	t3 * (m)	t (m)
Spudcan (Visualising)	6	1.35	0.86	1.40	0.35	0.15
Flat (Visualising)	6	1.35	-	-	-	1.0
Spudcan (Non-visualising)	6	2.92	0.86	1.40	0.35	0.30
	8	2.92	1.15	1.87	0.58	0.30
	10	2.92	1.44	2.33	0.81	0.30
	12	2.92	1.44	2.80	1.07	0.30
	14	2.92	2.02	3.27	1.27	0.30
	16	2.92	2.30	3.73	1.50	0.30
Flat (Non-visualising) : Cylindrical curvature on underside of 420 mm radius	6	2.92	-	-	-	0.55
	12	2.92	-	-	-	1.19
	16	2.92	-	-	-	1.42

* The geometric parameters D, d_s, t1, t2 & t3 are defined in Figure 2.

Table 2: Details of test geometries and soil properties (all tests conducted at 200 g).

Test*	H_{ct} (m)	H_s (m)	D (m)	H_{ct}/D (-)	H_s/D (-)	s_{um} (kPa)	ρ_{ct} (kPa/m)	s_{ubi} (kPa)	ρ_{cb} (kPa/m)	φ_{cv} (°)	I_D (%)	γ'_s (kN/m^3)	γ'_{ct}** (kN/m^3)	γ'_{cb}** (kN/m^3)	υ (mm/s)	Remarks
T1SP	2.38	4	6	0.40	0.67	4.9	1.9	25.6	2.5	31	74	10.6	6.85	7.32	0.254	PIV visualising tests
T2SP	4.32	4	6	0.72	0.67	4.5	1.6	27	2.5	31	74	10.6	6.85	7.32	0.254	
T3SP	5.47	4	6	0.91	0.67	4.1	1.5	26	2.3	31	74	10.6	6.85	7.32	0.254	
T4SP	0	4	6	0.00	0.67	0	0	18.7	2	31	74	10.6	6.85	7.32	0.254	
T5SP	3.44	2	6	0.57	0.33	4.7	1.7	18.2	2	31	74	10.6	6.85	7.32	0.254	
T6SP	4.35	6	6	0.72	1.00	4.5	1.6	26	2.3	31	74	10.6	6.85	7.32	0.254	
T1FL	2.35	4	6	0.39	0.67	4.9	1.9	25.6	2.5	31	74	10.6	6.85	7.32	0.254	
T2FL	4.01	4	6	0.67	0.67	4.5	1.6	26.7	2.5	31	74	10.6	6.85	7.32	0.254	
T3FL	5.10	4	6	0.85	0.67	4.1	1.5	25.8	2.3	31	74	10.6	6.85	7.32	0.254	
T4FL	0	4	6	0.00	0.67	0	0	18.7	2	31	74	10.6	6.85	7.32	0.254	
T5FL	3.36	2	6	0.56	0.33	4.8	1.7	18.1	2	31	74	10.6	6.85	7.32	0.254	
T6FL	4.05	6	6	0.68	1.00	4.5	1.6	26	2.3	31	74	10.6	6.85	7.32	0.254	
SPa16	6.42	6.25	16	0.40	0.39	0.2	0.5	22.6	2.2	31	51	10.14	6.61	7.63	0.095	Full drum tests: Section-a
SPa14	6.42	6.25	14	0.46	0.45	0.2	0.5	22.6	2.2	31	51	10.14	6.61	7.63	0.109	
SPa12	6.42	6.25	12	0.54	0.52	0.2	0.5	22.6	2.2	31	51	10.14	6.61	7.63	0.127	
SPa10	6.42	6.25	10	0.64	0.63	0.2	0.5	22.6	2.2	31	51	10.14	6.61	7.63	0.152	
SPa6	6.42	6.25	6	1.07	1.04	0.2	0.5	22.6	2.2	31	51	10.14	6.61	7.63	0.254	
FLa6	6.42	6.25	6	1.07	1.04	0.2	0.5	22.6	2.2	31	51	10.14	6.61	7.63	0.254	
SPb16	6.32	4	16	0.39	0.25	0.2	0.5	24.6	2.4	31	51	10.14	6.61	7.63	0.095	Full drum tests: Section-b
SPb12	6.32	4	12	0.53	0.33	0.2	0.5	24.6	2.4	31	51	10.14	6.61	7.63	0.127	
SPb8	6.32	4	8	0.79	0.50	0.2	0.5	24.6	2.4	31	51	10.14	6.61	7.63	0.190	
SPb6	6.32	4	6	1.05	0.67	0.2	0.5	24.6	2.4	31	51	10.14	6.61	7.63	0.254	
FLb12	6.32	4	12	0.53	0.33	0.2	0.5	24.6	2.4	31	51	10.14	6.61	7.63	0.127	
SPc16	4	4	16	0.25	0.25	0.3	0.58	23	2.5	31	51	10.14	6.61	7.63	0.095	Full drum tests: Section-c
SPc8	4	4	8	0.50	0.50	0.3	0.58	23	2.5	31	51	10.14	6.61	7.63	0.190	
SPc6	4	4	6	0.67	0.67	0.3	0.58	23	2.5	31	51	10.14	6.61	7.63	0.254	
FLc16	4	4	16	0.25	0.25	0.3	0.58	23	2.5	31	51	10.14	6.61	7.63	0.095	

* SP=Spudcan; FL=Flat; a, b, c represents the three sections of the drum centrifuge respectively; ** based on average moisture content

Journal: **Geotechnique**
Article number: **16-P-100R1**
Title: **Foundation punch-through in clay with sand: centrifuge modelling**
Author(s): **Shah Neyamat Ullah, PhD; Samuel Stanier, PhD; Yuxia Hu, PhD; David White, PhD**
Article type: **General Paper**

Note: All changes made to the manuscript in this revision have been highlighted in purple in the revised manuscript.

<table>
<tr><th>Review 2 comments</th><th>Authors reply</th></tr>
<tr><td>General comments

The paper is clearly written and addresses an important issue with regards the safety of offshore jack up rigs and punch-through predictions. This work then is developed to create a design methodology in the companion paper.
The main area where the reviewer requires further reassurance is in the verification that boundary affects (base) do not interfere with the results of the study. The significant rate of increase in bearing pressure seen towards the end of the test in Figure 3 (which seems increased for the flat foundation as would be anticipated) and the increased bearing pressures over industry experience suggest that this point is considered further. The authors fail to consider that effectively the travelling plug of soil has extended the depth of the foundation by 1.12D and thus it is unclear if the boundary interaction is most critical for the base of the foundation or the plug of material. Some further consideration or reassurance is necessary here. Maybe this is considered in response and the reviewer has misunderstood or it is covered in the additional papers referenced. If the latter case, more detailed statements of this consideration should be added here (i.e. extracts from text in the papers). Could this issue not easily be dealt with via a simple FEA simulation where a foundation shape is created that includes the plug of soil below</td><td>We thank the reviewer for taking the time to re-review our paper, and we have endeavoured below to provide further reassurance regarding potential boundary effects. We agree that it is important to lay this issue to rest, particularly since our conclusions may potentially become adopted in practice.

The FEA simulation the reviewer proposes has already been conducted using large deformation finite element methods, as reported in Ullah et al. (2014), which is referenced on pages 5-6 of the revised version. In our previous reply we provided example calculations using the expressions derived from the FEA simulations that were reported by Ullah et al. (2014). For clarity we will provide a more comprehensive summary of those calculations here.

Bottom boundary effect:

The governing equation to conservatively define the depth of the bottom boundary affected zone in spudcan penetration tests, as proposed by Ullah et al. (2014), is as follows:

$$d_{BE} = (0.4*(H_{plug}/D) + 0.7)*D$$

where H_{plug} is the composite height of the foundation and plug, D is the foundation diameter and d_{BE} is the depth of the boundary affected zone. This is the minimum distance from the spudcan to the base of the container to avoid bottom boundary effects. d_{BE} is taken from the base of the sample to the load reference point on the foundation (taken in all our tests as the lowest depth of maximal projected area). The expression implicitly accounts for the height of the plug of soil entrapped beneath the foundation that is of concern to the reviewer. The original LDFE study that was used to derive this relationship explored bottom boundary effects in sand-clay stratigraphies. For the clay-sand-clay stratigraphies reported in this manuscript, we conservatively assume that 100% of the sand layer height becomes entrapped beneath the foundation, along with 7% of the top clay layer height (estimated from the images recorded in the visualising tests).</td></tr>
</table>

the foundation as part of the foundation (simplistic I realise as soil plug properties may be interesting in reality).

Again I would urge further consideration of the following (as raised previously). The reviewer notes that both papers are very definitive and confident in their findings. As the papers may form the basis of new design methods the authors are urged to point out any limitations of their findings and scope of work and add appropriate caveats so that if the methods do find their way into industrial design practice they are used appropriately and do not lead to dangerous situations. For example, does the range of sand densities investigated mean that the findings can be applied globally? This latter specific point seems to have been ignored in the response to reviewers.

The plot below compares this limit d_{BE} with the geometries and final spudcan depths of the two sets of tests. This includes both the 'visualising' tests in a small windowed strongbox within the drum centrifuge channel with 16 m lower clay layer depth and 'non-visualising' tests within the drum centrifuge channel itself with 24 m lower clay layer depth. The final depth is the last recorded measurement prior to extraction, and the distance from this point to the bottom boundary is d_{AS}. Again, this was calculated with respect to the load reference point on the foundation rather than at the depth of the base of the entrapped plug of soil, so as to be consistent with the bottom boundary effect estimation method proposed in Ullah et al. (2014). d_{AS} and d_{BE} are compared in the plot below.

There is no bottom boundary effect so long as the depth of available space, d_{AS}, is greater than the depth of the boundary affected zone, d_{BE}. Figure 1 illustrates that this was the case for all of the tests we report in this manuscript.

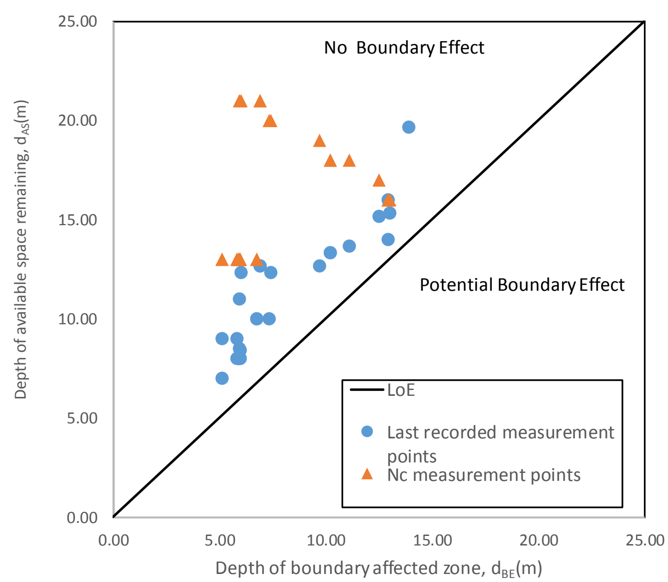

Figure 1: Graphical summary of potential bottom boundary effect in new centrifuge tests reported.

Further to that, the bottom boundary is most likely to influence the deep penetration resistance in the lower clay layer, from which the bearing capacity factors, N_c, are calculated. In this paper these factors were back-calculated at the point at which the load reference point on the foundation had penetrated 0.5D into the lower clay layer, following Hu et al. (2014). This depth was typically significantly less than the depth at which the test was terminated (and at which the potential bottom boundary effects were assessed in Figure 1), meaning that any influence of bottom boundary effects on the analytical model developed in the companion paper is even less likely.

Lateral boundary effect:

For the lateral boundary effects we can simply plot the geometry of each of the experiments reported on the design chart published in Ullah et al. (2016b), as illustrated in Figure 2 (relevant tests represented by blue diamonds). The two curves bounding the grey shaded region reflect the minimal lateral boundary distance required for there to be minimal influence (<5%) on the measured penetration resistance due to lateral boundary proximity for rough (upper) and smooth (lower) sidewall boundary conditions, respectively. Given that the sidewalls of our strongboxes were greased prior to sample preparation to aid consolidation in-flight, we conclude that there is likely minimal lateral boundary effect for all of the tests reported.

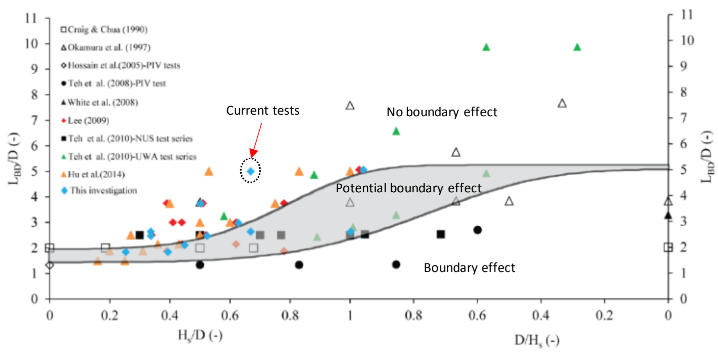

Figure 2: Graphical summary of potential lateral boundary effect in new centrifuge tests reported, after Ullah et al. (2016).

We hope the above two figures – derived from a significant number of large deformation finite element analyses - are sufficient to alleviate the reviewer's concerns about the potential for boundary effects influencing the experimental measurements. In the revised manuscript – for brevity – we only state that bottom and lateral strongbox boundary effects were avoided based on the criteria proposed in Ullah et al. (2014, 2016b).

	Model limitations: The effect of sand density is inherently catered for in our model through the modified strength-dilatancy relationships of Bolton (1986), with excellent model performance evident for both medium dense and dense sand for the new clay-sand-clay cases. However, at the reviewer’s suggestion we have outlined the limitations of our study in point 5 of the conclusion and the abstract of the companion paper.
Detailed comments 1. Experimental procedure Page 5, para 1, lines 42 & 53, suggest the foundations were penetrated to depths typically greater than those given in the response to reviewer's comments with respect to boundary effects. Stating that you got within 1D is not particularly reassuring. The reviewer still has some concerns about base boundary effects which would be mitigated to some extent if it was made clear in the paper at what actual depths (relative to the base) at which Nc was determined (as mentioned in your response to reviewers) rather than stating the foundation got within 1D of the box base. The reviewer is a little concerned about the defence of base boundary separation adopted if this has been understood correctly. To avoid boundary effects the reviewer would assume you would need at least 1D of unaffected material below that which is moving (ie D+1.12D) as the material trapped below the foundation is effectively forming part of (and moving with) the foundation and thus effectively increases the depth of the foundation by 1.12D. Based upon my understanding of the explanation given this suggests only 0.55D clear space under the foundation plus trapped soil at the end of the test. Note the references added on page 5 & 6 with regards boundary effects do	 As outlined in the response to the previous comment, the boundary affected zone is estimated from the base of the foundation and not from the base of the plug (following Figure 1 in Ullah et al. 2014). Hopefully the explanation given in response to the previous comment is now sufficient to alleviate the reviewer’s concerns regarding the potential for boundary effects influencing the experimental measurements and analytical model development. The references of page 5 and 6 have now been added.

not appear in the reference list	
2. Model geometries Page 6, para 1, line 39, Is a another bracket required after reference?	Bracket has been added.
Soil properties 3. Page 7, para 1, line7-10, Floating sentence seems strange and should be integrated with the rest of the paragraph.	This sentence has been integrated as suggested.
Load penetration responses… 4. Page 8, para 2, line 48-49, "once more -once when" doesn't read well, revisit.	The latter 'once' has been removed.
Peak failure mechanisms 5. Page 11, para 2, line 45-46, suggest replace "relation" with "relationship". Similar on page 12, line 2-3.	Replaced as suggested.
6. Bearing capacity mechanism in the … Page 14, para 3, line 44-45, A typical range of Ks values has been shown. It would be useful to know what value was adopted here based upon the phi cv where Ks can also vary with q2/q1. This comment also applies to page 16	The Ks values are taken here from the ISO chart. q2 and q1 represent the conventional shallow bearing capacity resistance as mentioned in the guidelines. We have omitted calculation of q1 and q2 for brevity; however, they could be readily calculated by readers, following the guidelines referenced.
7. Page 16, line 1-3, As per above as it is unclear what values were adopted earlier it is not clear what are considered very high values. Without such it is difficult to make the statement on line 3.	On page 14 we have discussed the projected angles employed by the industry guidelines. Hence higher values mean higher than those recommended values (~11-18^{o}). This is now mentioned explicitly in the text on page 16.
8. Page 16, line 42-43, reference is made to blue marker, not clear I this is figure here (wouldn't this be in black and white) or in ISO.	Test T3SP is blue marked and also indicated by an arrow in Figure 14, Figure 15 and Figure 16 to highlight the beneficial effect of the compensating errors (i.e. under predictions of q_{peak} and N_c lead to reasonable estimates of d_{punch}). Evidently, this point needs to be identified in all three figures (14-16) for clarity.
9. References	

Check missing references referred to earlier. Several papers seem to be missing page numbers and complete references. Some papers see to have numbers, are these DOI as not clear and should be pre-fixed by DOI. If in print update with relevant numbers and page numbers etc.	The missing references have been added. The missing page numbers have also been added. The numbers referred to are digital paper numbers rather than DOIs.
10. Figures Figure 8 & 9 caption text. "for within a" does not read well, revise.	This has been revised by deleting the word ‘within’.

Reviewer #2: The Authors have systematically answered the Reviewers Comments. In this new version of the paper the experimental process (soil preparation, soil properties experimental details etc) is described in more detail. The typos and some confusing phrasing have been corrected. Overall the modifications made the paper stronger and easier to follow.	We thank the reviewer for taking the time to re-review our paper.

References:

Ullah, S.N., Hu,Y., Stanier, S. A. & White, D. J. (2014). LDFE study of bottom boundary effect in foundation model tests. *International Journal of Physical Modelling in Geotechnics* **14(3)**, 80-87

Ullah, S.N., Hu,Y., Stanier, S. A. & White, D. J. (2016b). Lateral boundary effects in centrifuge foundation tests. *International Journal of Physical Modelling in Geotechnics,* available online ahead of print.

Copyright Form

ice
Institution of Civil Engineers
publishing

Journal Publishing Agreement

It is our policy to ask authors to assign the copyright of articles accepted for publication to the Publisher. Exceptions are possible for reasons of national rules or funding. Please tick the relevant options below.

In assigning copyright to us, you retain all proprietary rights including patent rights, and the right to make personal (non-commercial) use of the article, subject to acknowledgement of the journal as the original source of publication.

By signing this agreement, you are confirming that you have obtained permission from any co-authors and advised them of this copyright transfer. Kindly note that copyright transfer is not applicable to authors who are opting to publish their papers as Open Access. Open Access authors retain copyright of their published paper.

Please complete the form below and return an electronic copy to your ICE Publishing contact: (http://www.icevirtuallibrary.com/info/submit).

Journal name: Géotechnique

Article title: Foundation punch-through in clay with sand: Centrifuge modelling

Manuscript reference number: 16-P-100R2

Authors: Shah Neyamat Ullah, Samuel Stanier, Yuxia Hu and David White

Your name: Shah Neyamat Ullah

Signature and date: NU. 21/11/2016

Please tick either one option from part A or one option from part B. Please complete part C.

A. Copyright

- [x] I hereby assign and transfer the copyright of this paper to Thomas Telford Ltd.
- [ ] British Crown Copyright: I hereby assign a non-exclusive licence to publish to Thomas Telford Ltd.
- [ ] I am a US Government employee: employed by (name of agency) ....
- [ ] I am subject to the national rules of (country) .... and confirm that I meet their requirements for copyright transfer or reproduction (please delete as appropriate)

B. Authors with open access funding requirements. Please specify the Creative Commons license version required.

- [ ] CC-BY (for full details click here Creative Commons Attribution (CC BY) 4.0 International License)
- [ ] CC-BY-NC-ND (for full details click here Creative Commons Attribution Non Commercial No-derivatives (CC BY NC ND) 4.0 International License)

C. Please confirm that you have obtained permission from the original copyright holder. For ICE Publishing's copyright policy, please click here. ICE Publishing is a signatory to the STM Guidelines.

- [ ] I have obtained permission from the original copyright holder for the use of all subsidiary material included in this paper (E.g. for borrowed figures or tables).

Fig 1

Click here to download Figure Figure 1.eps

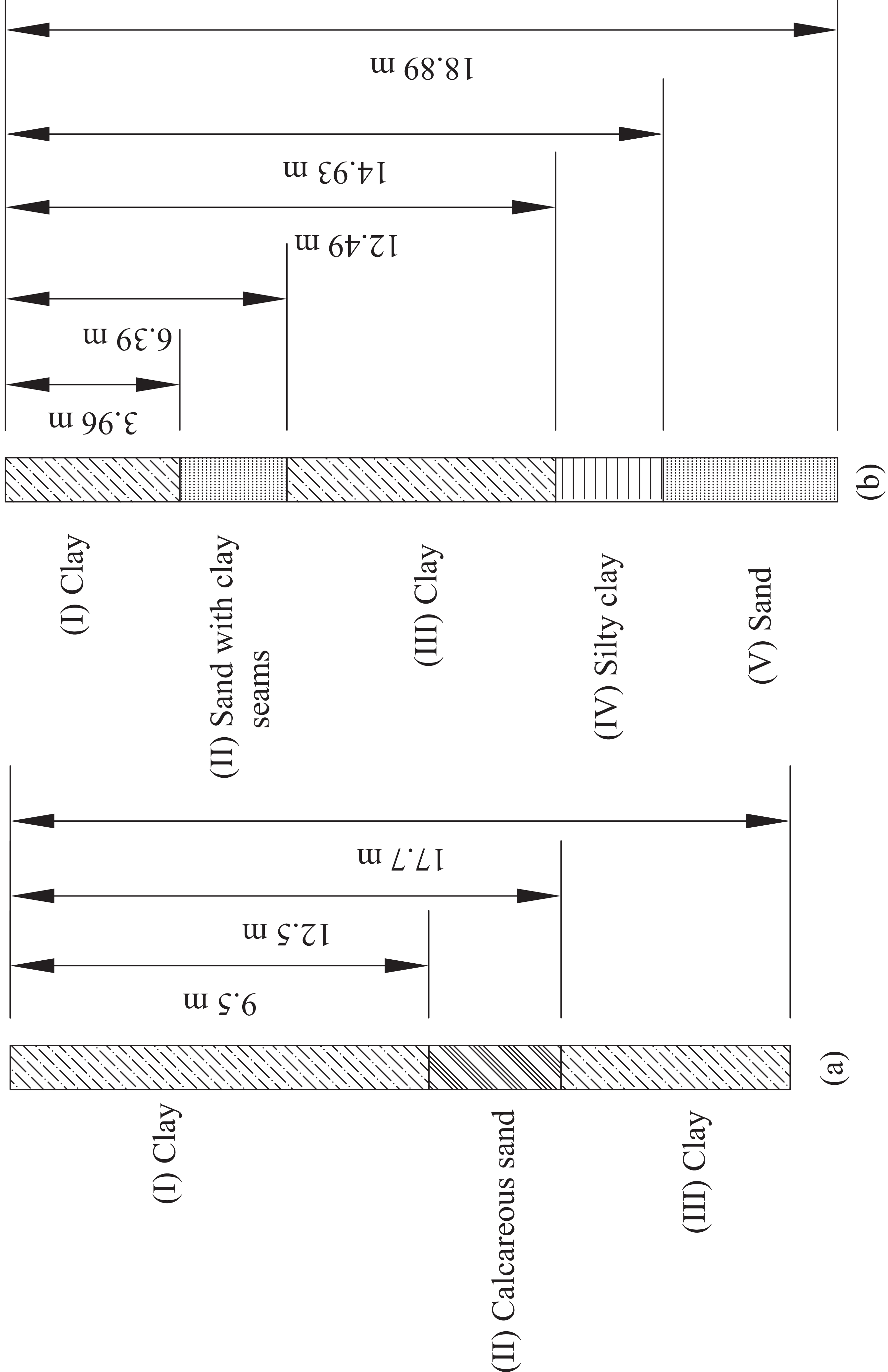

Fig 2

Click here to download Figure Figure 2.eps

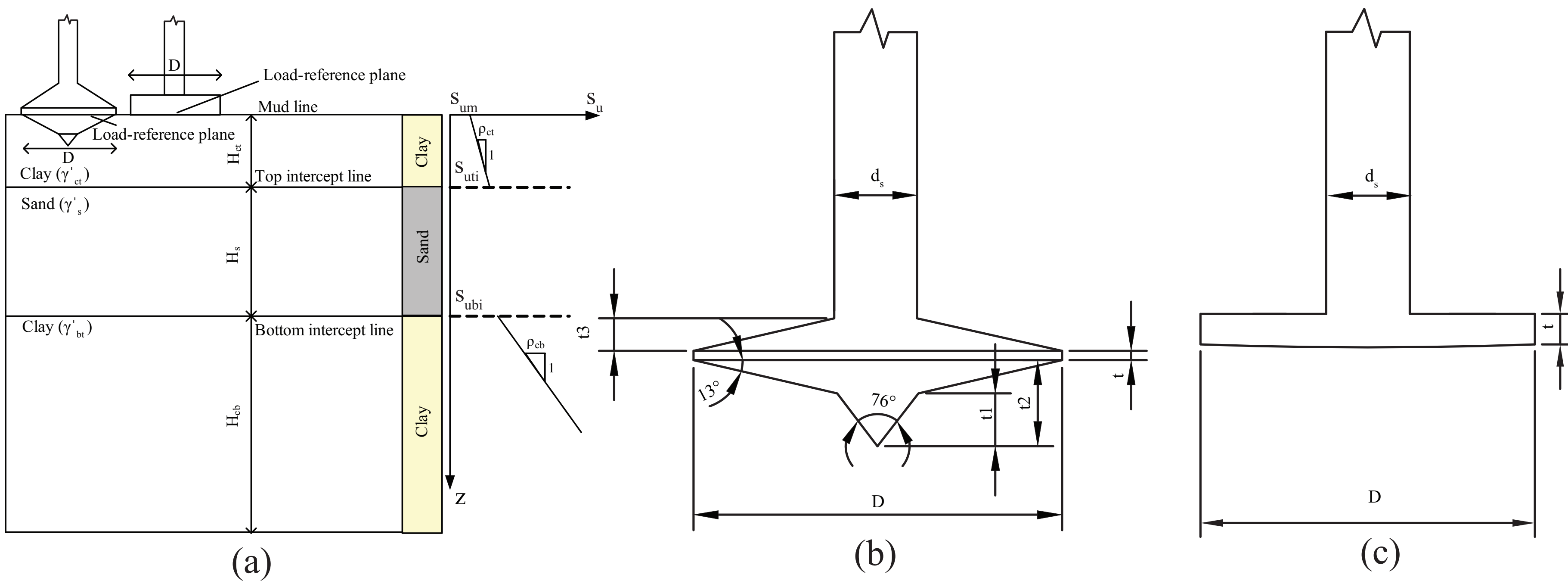

Fig 3

Click here to download Figure Figure 3.eps

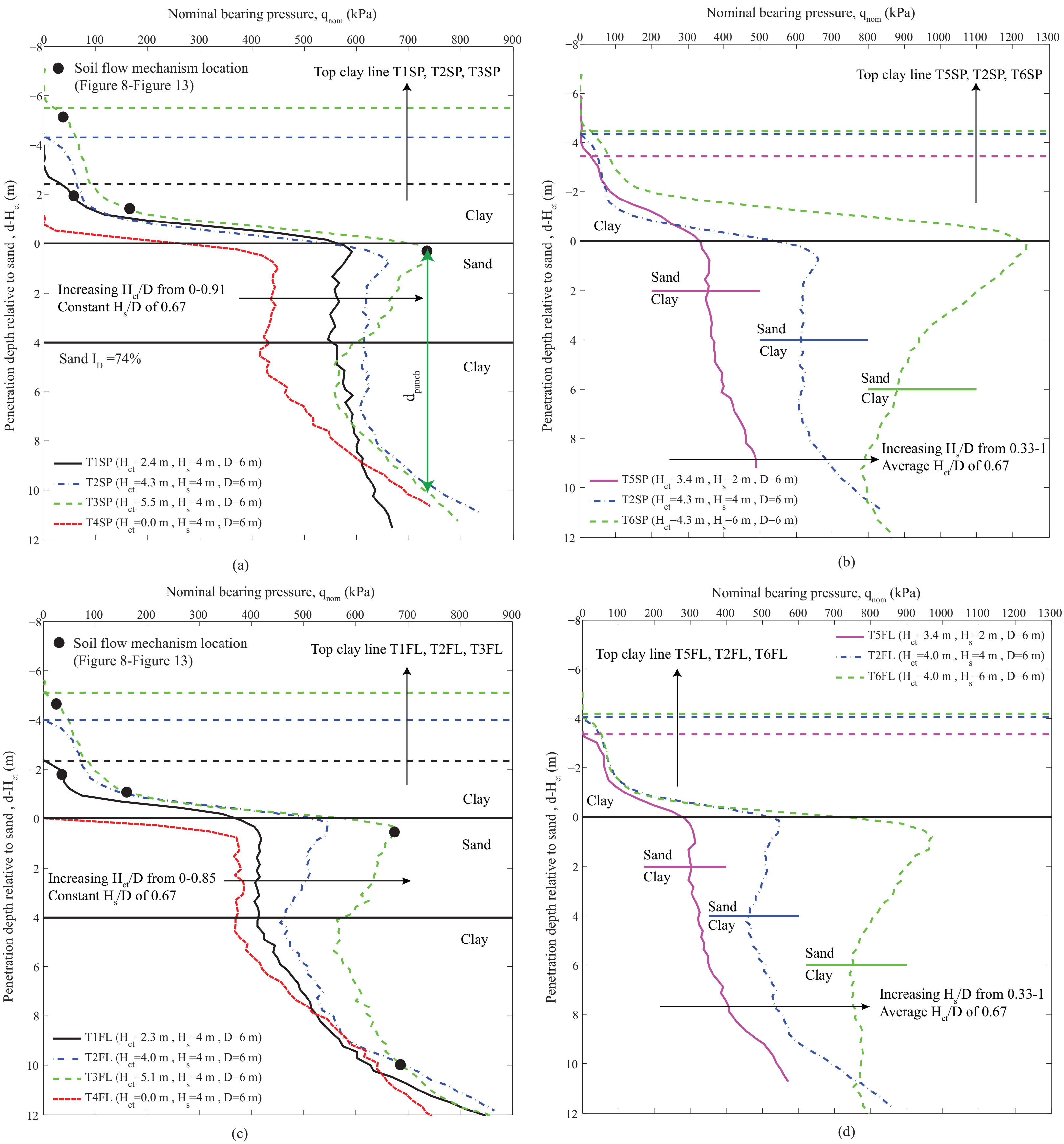

Fig 4

Click here to download Figure Figure 4.eps

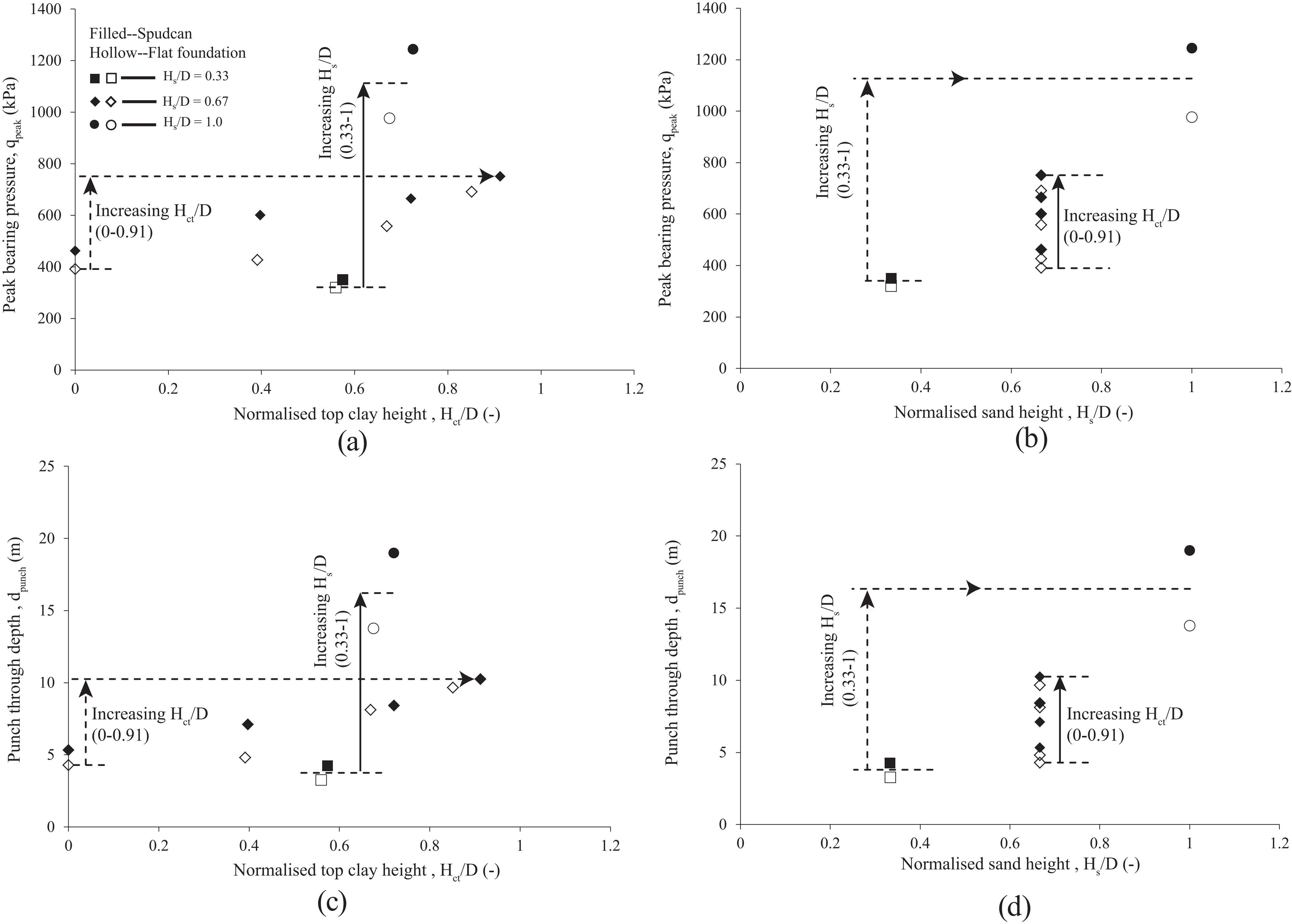

Fig 5

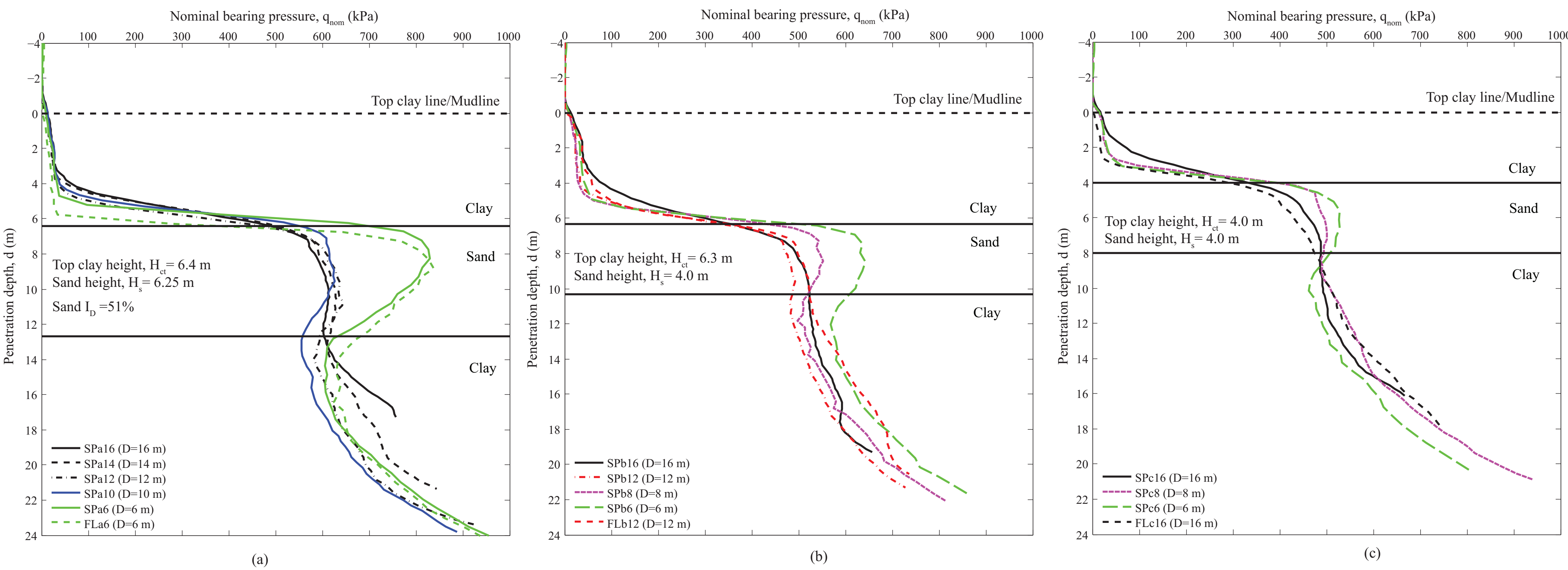
Nominal bearing pressure, q_{nom} (kPa)
Penetration depth, d (m)
Top clay line/Mudline
Clay
Sand
Clay
Top clay height, H_{ct} = 6.4 m
Sand height, H_s = 6.25 m
Sand I_D =51%
SPa16 (D=16 m)
SPa14 (D=14 m)
SPa12 (D=12 m)
SPa10 (D=10 m)
SPa6 (D=6 m)
FLa6 (D=6 m)
(a)
Nominal bearing pressure, q_{nom} (kPa)
Penetration depth, d (m)
Top clay line/Mudline
Clay
Sand
Clay
Top clay height, H_{ct} = 6.3 m
Sand height, H_s = 4.0 m
SPb16 (D=16 m)
SPb12 (D=12 m)
SPb8 (D=8 m)
SPb6 (D=6 m)
FLb12 (D=12 m)
(b)
Nominal bearing pressure, q_{nom} (kPa)
Penetration depth, d (m)
Top clay line/Mudline
Clay
Sand
Clay
Top clay height, H_{ct} = 4.0 m
Sand height, H_s = 4.0 m
SPc16 (D=16 m)
SPc8 (D=8 m)
SPc6 (D=6 m)
FLc16 (D=16 m)
(c)

Fig 6

Click here to download Figure Figure 6.eps

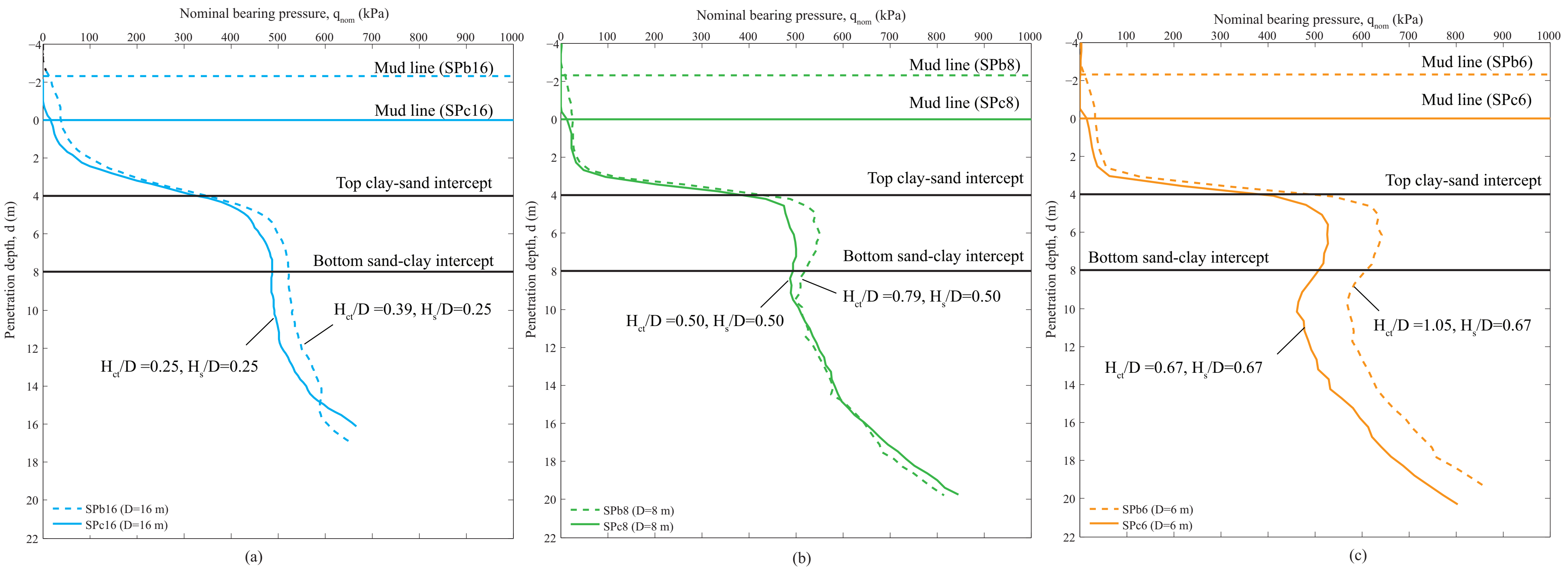

Fig 7

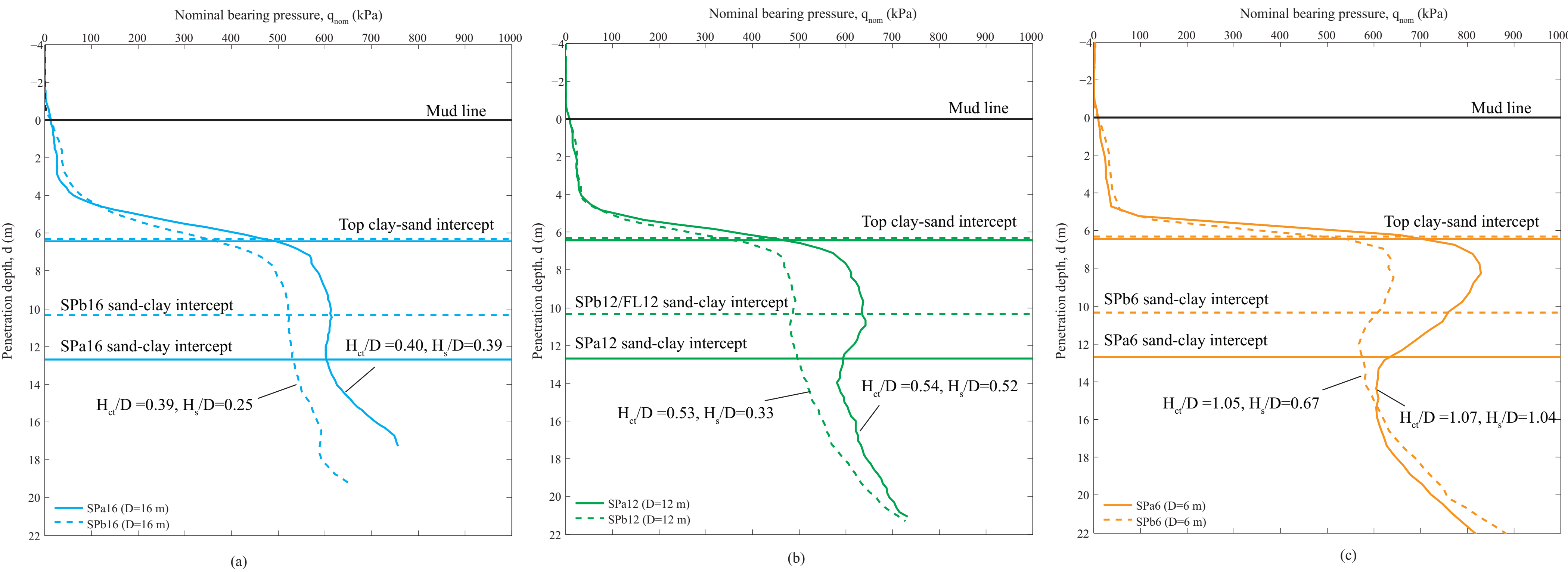
Nominal bearing pressure, q_nom (kPa)
Penetration depth, d (m)
Mud line
Top clay-sand intercept
SPb16 sand-clay intercept
SPa16 sand-clay intercept
H_ct/D =0.40, H_s/D=0.39
H_ct/D =0.39, H_s/D=0.25
SPa16 (D=16 m)
SPb16 (D=16 m)
(a)
SPb12/FL12 sand-clay intercept
SPa12 sand-clay intercept
H_ct/D =0.54, H_s/D=0.52
H_ct/D =0.53, H_s/D=0.33
SPa12 (D=12 m)
SPb12 (D=12 m)
(b)
SPb6 sand-clay intercept
SPa6 sand-clay intercept
H_ct/D =1.05, H_s/D=0.67
H_ct/D =1.07, H_s/D=1.04
SPa6 (D=6 m)
SPb6 (D=6 m)
(c)

Fig 8

Click here to download Figure Figure 8.eps

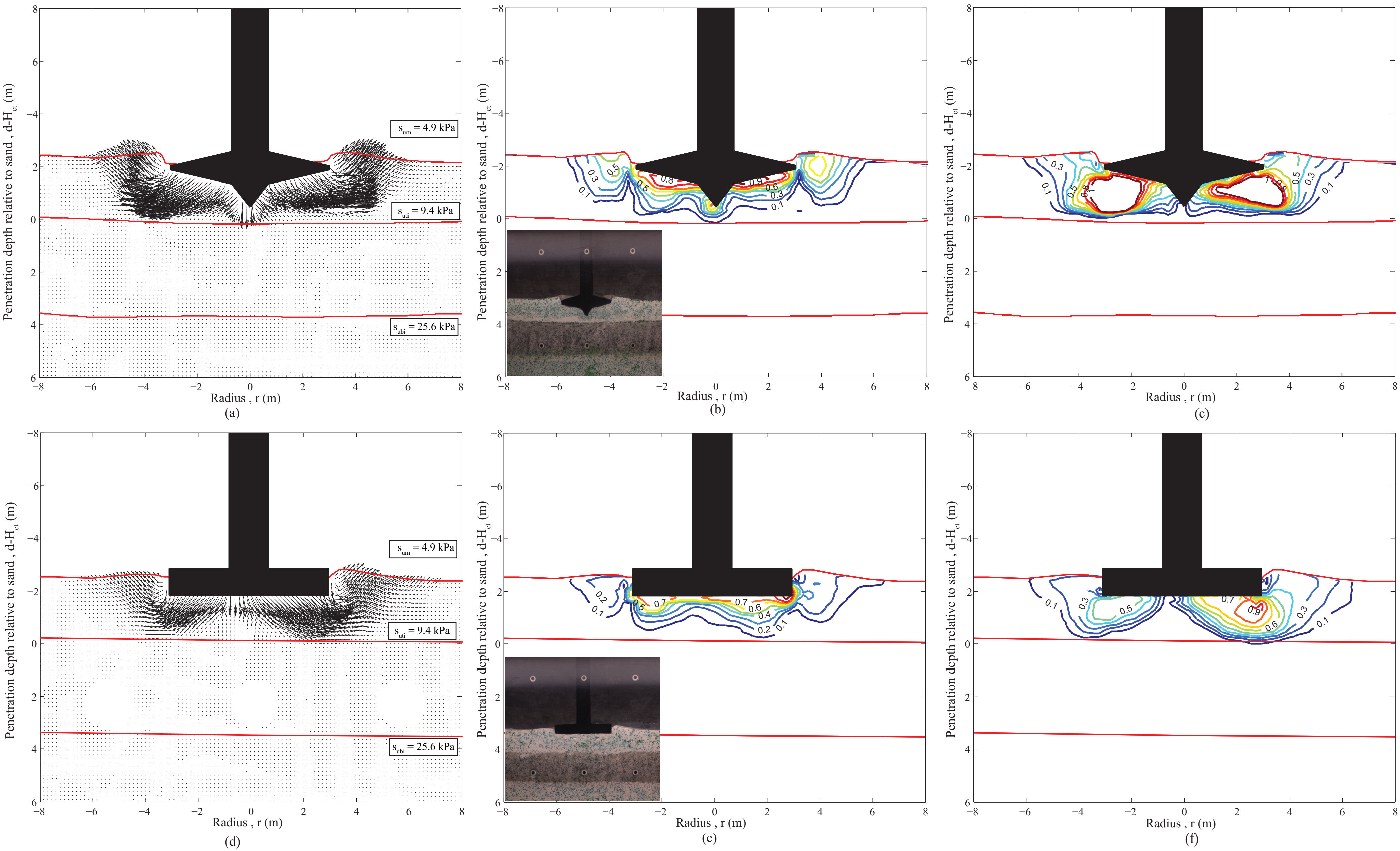

Fig 9 Click here to download Figure Figure 9.eps

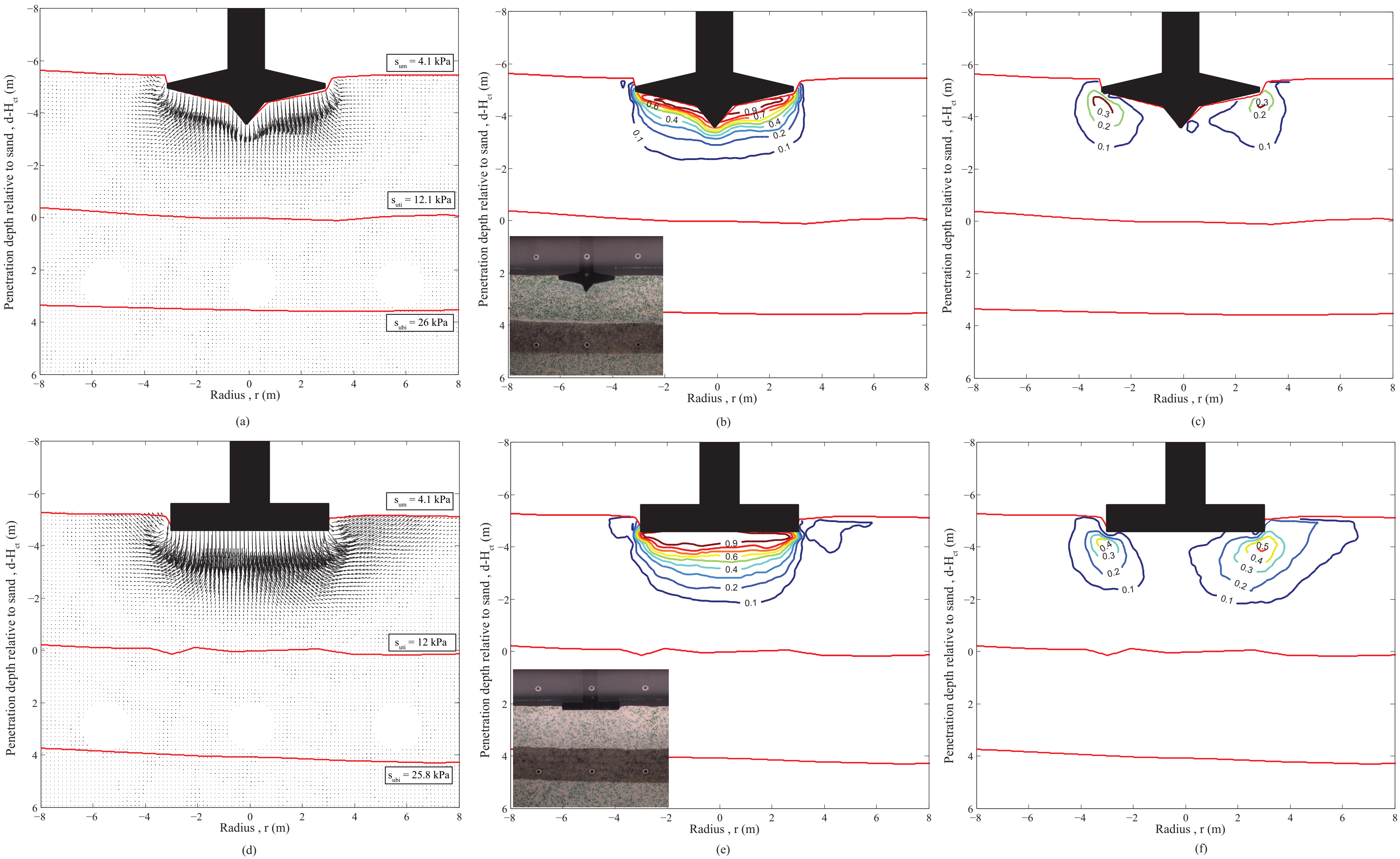

Fig 10

Click here to download Figure Figure 10 .eps

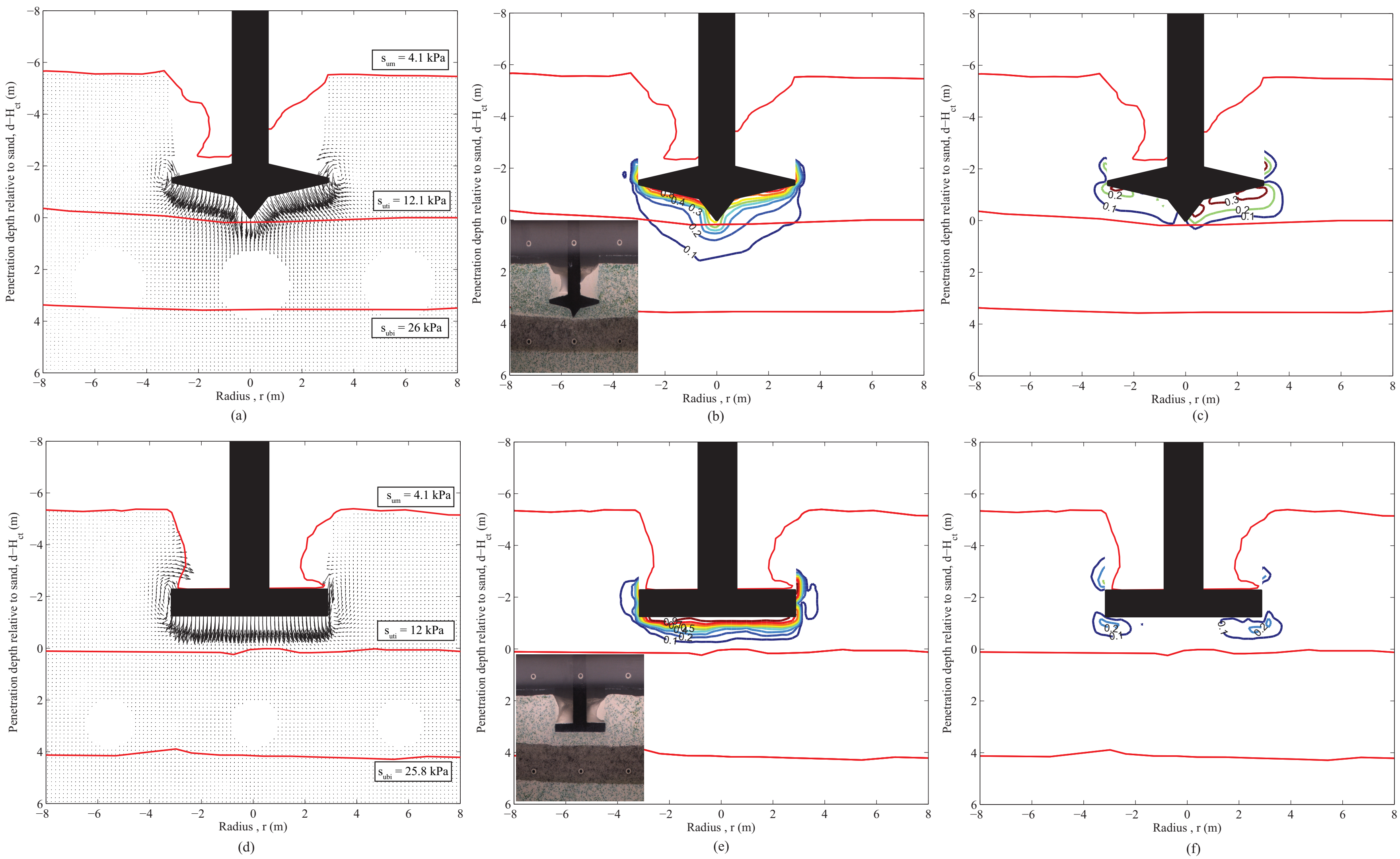

Fig 11

Click here to download Figure Figure 11 .eps

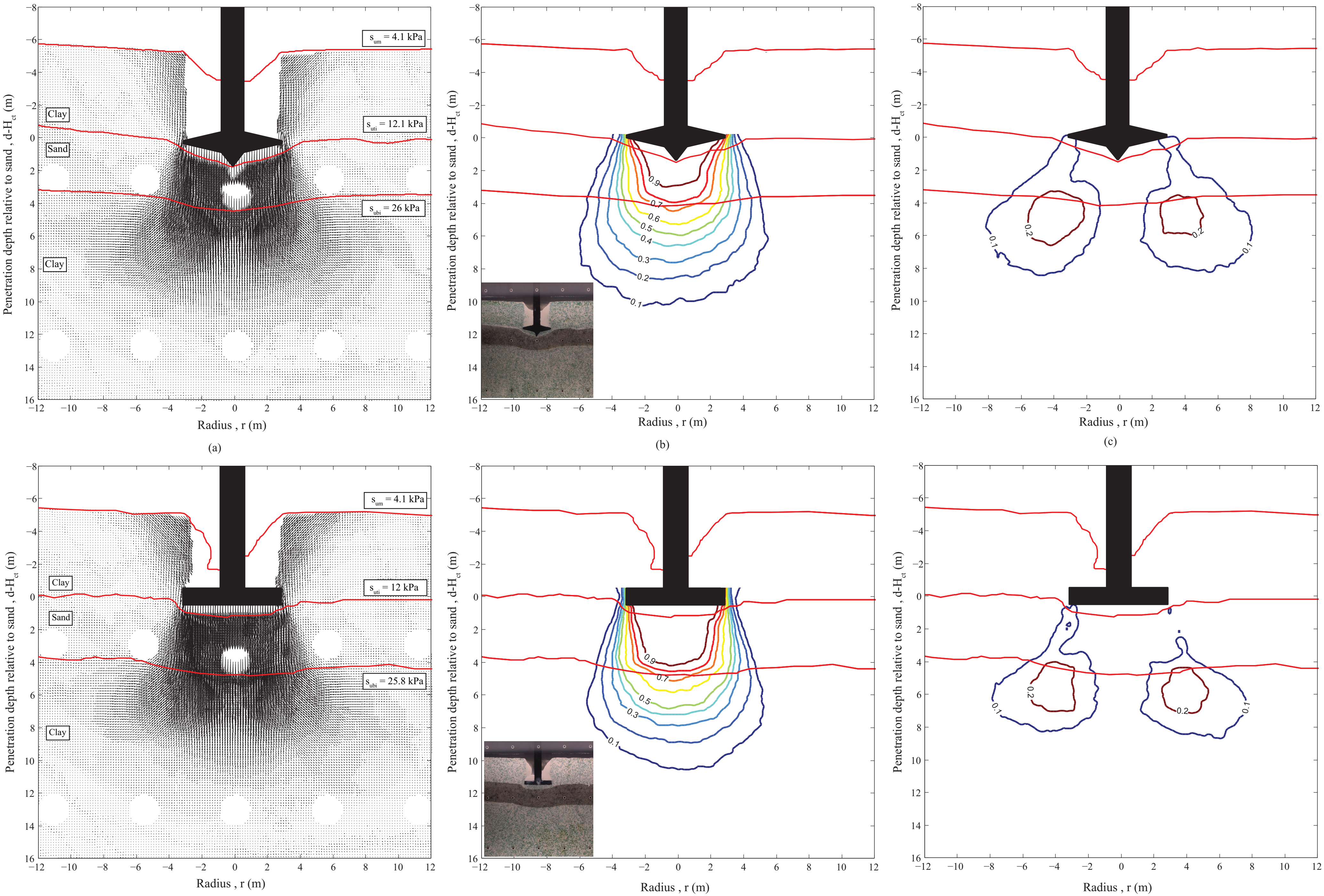

(a) (b) (c)

(d) (e) (f)

Fig 12

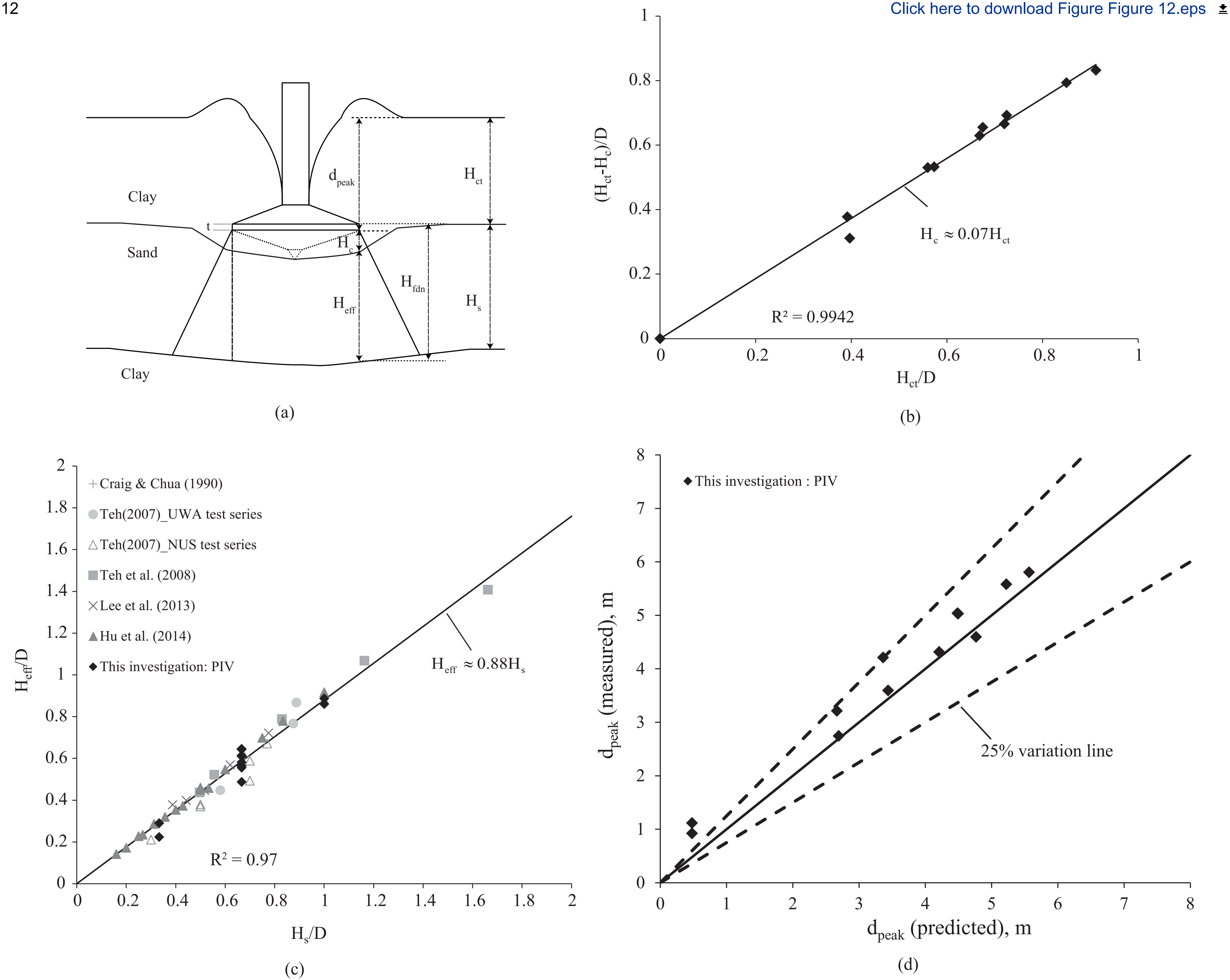

Clay
Sand
Clay
t
d_{peak}
H_{ct}
H_c
H_{eff}
H_{fdn}
H_s
(a)
$(H_{ct}-H_c)/D$
H_{ct}/D
$H_c \approx 0.07H_{ct}$
$R^2 = 0.9942$
(b)
H_{eff}/D
H_s/D
Craig & Chua (1990)
Teh(2007)_UWA test series
Teh(2007)_NUS test series
Teh et al. (2008)
Lee et al. (2013)
Hu et al. (2014)
This investigation: PIV
$H_{eff} \approx 0.88H_s$
$R^2 = 0.97$
(c)
d_{peak} (measured), m
d_{peak} (predicted), m
This investigation : PIV
25% variation line
(d)

Fig 13

Click here to download Figure Figure 13.eps

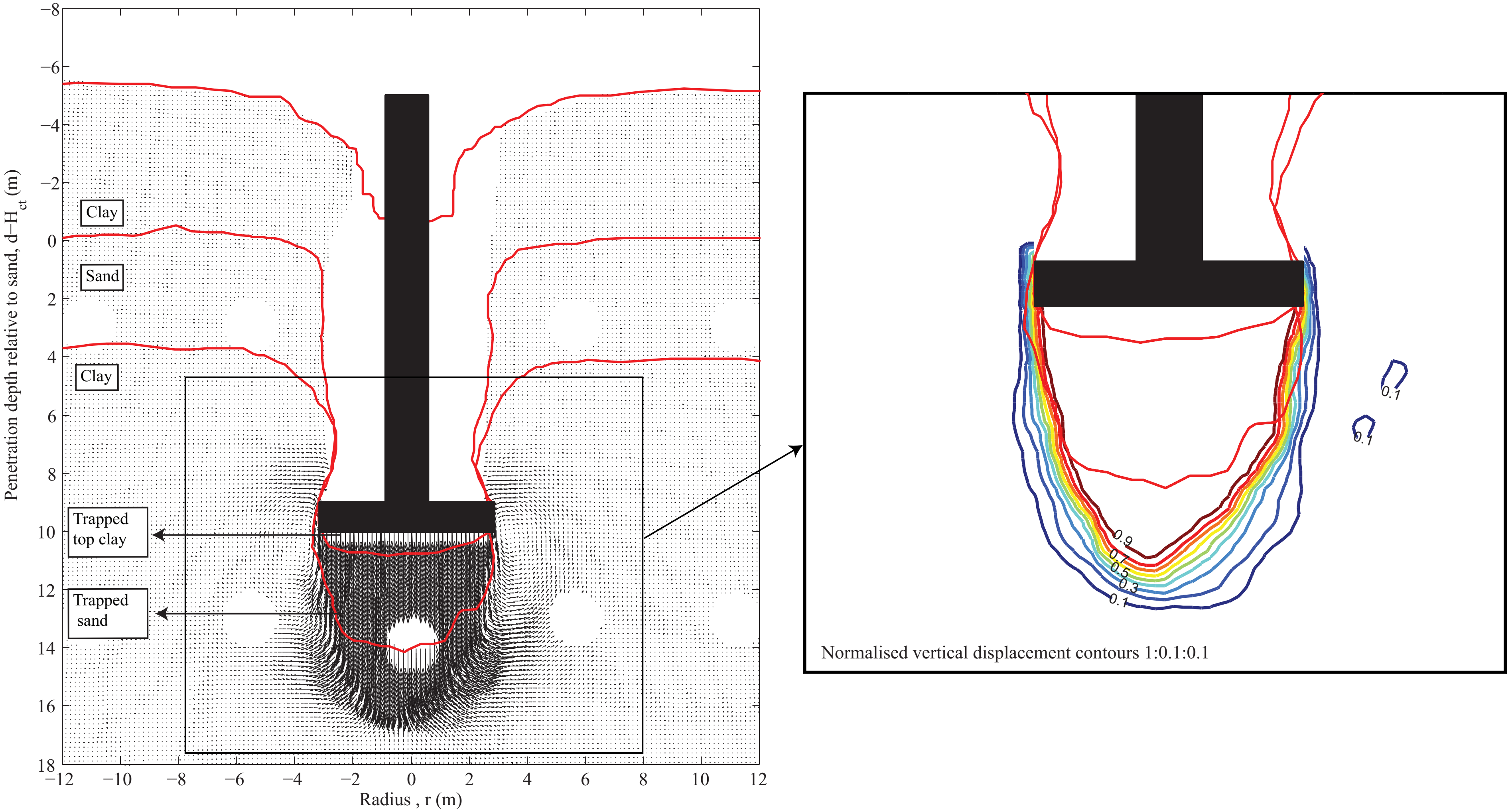

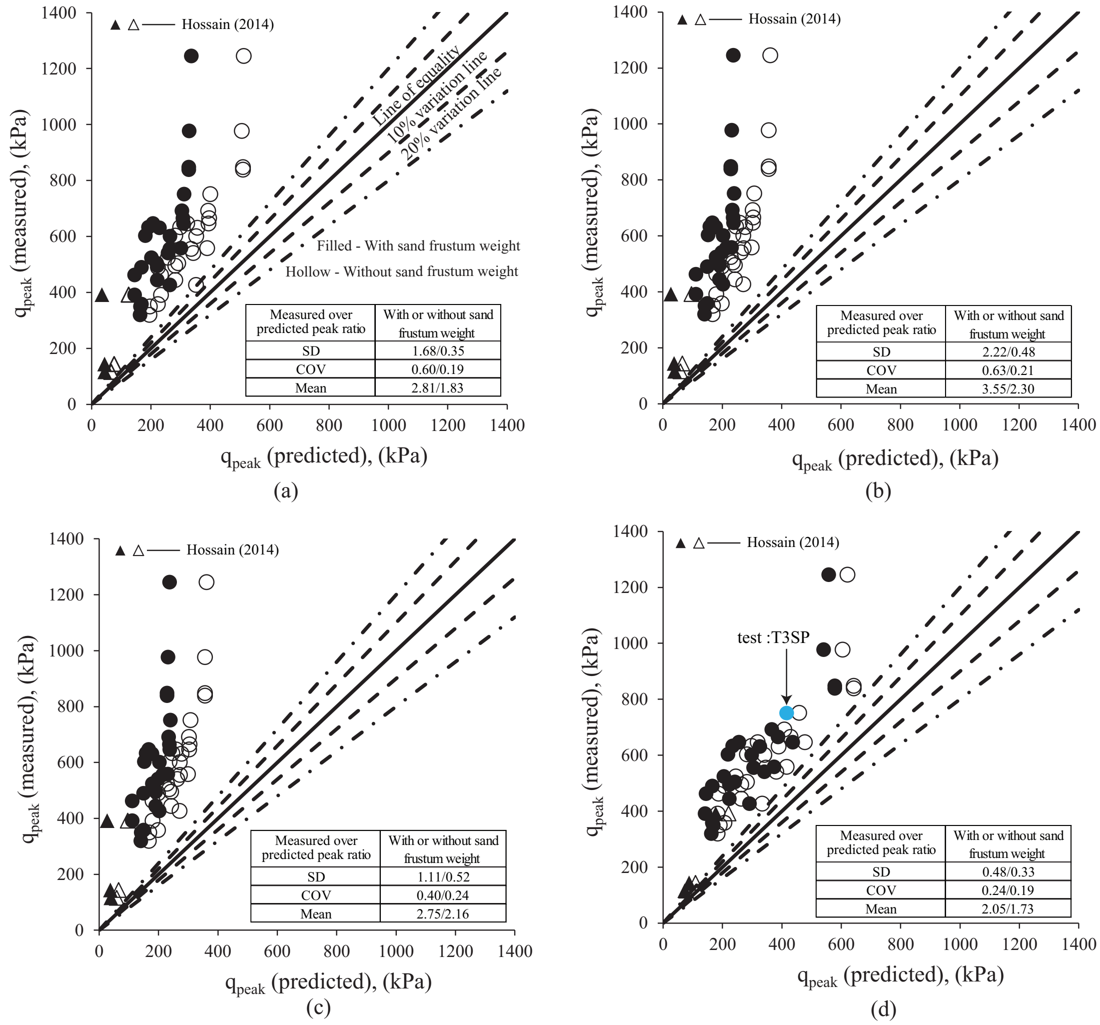
Hossain (2014)
Line of equality
10% variation line
20% variation line
Filled - With sand frustum weight
Hollow - Without sand frustum weight
Measured over predicted peak ratio | With or without sand frustum weight
SD | 1.68/0.35
COV | 0.60/0.19
Mean | 2.81/1.83
q_{peak} (measured), (kPa)
q_{peak} (predicted), (kPa)
(a)
Hossain (2014)
Measured over predicted peak ratio | With or without sand frustum weight
SD | 2.22/0.48
COV | 0.63/0.21
Mean | 3.55/2.30
q_{peak} (measured), (kPa)
q_{peak} (predicted), (kPa)
(b)
Hossain (2014)
Measured over predicted peak ratio | With or without sand frustum weight
SD | 1.11/0.52
COV | 0.40/0.24
Mean | 2.75/2.16
q_{peak} (measured), (kPa)
q_{peak} (predicted), (kPa)
(c)
Hossain (2014)
test :T3SP
Measured over predicted peak ratio | With or without sand frustum weight
SD | 0.48/0.33
COV | 0.24/0.19
Mean | 2.05/1.73
q_{peak} (measured), (kPa)
q_{peak} (predicted), (kPa)
(d)

Fig 15

Click here to download Figure Figure 15.eps

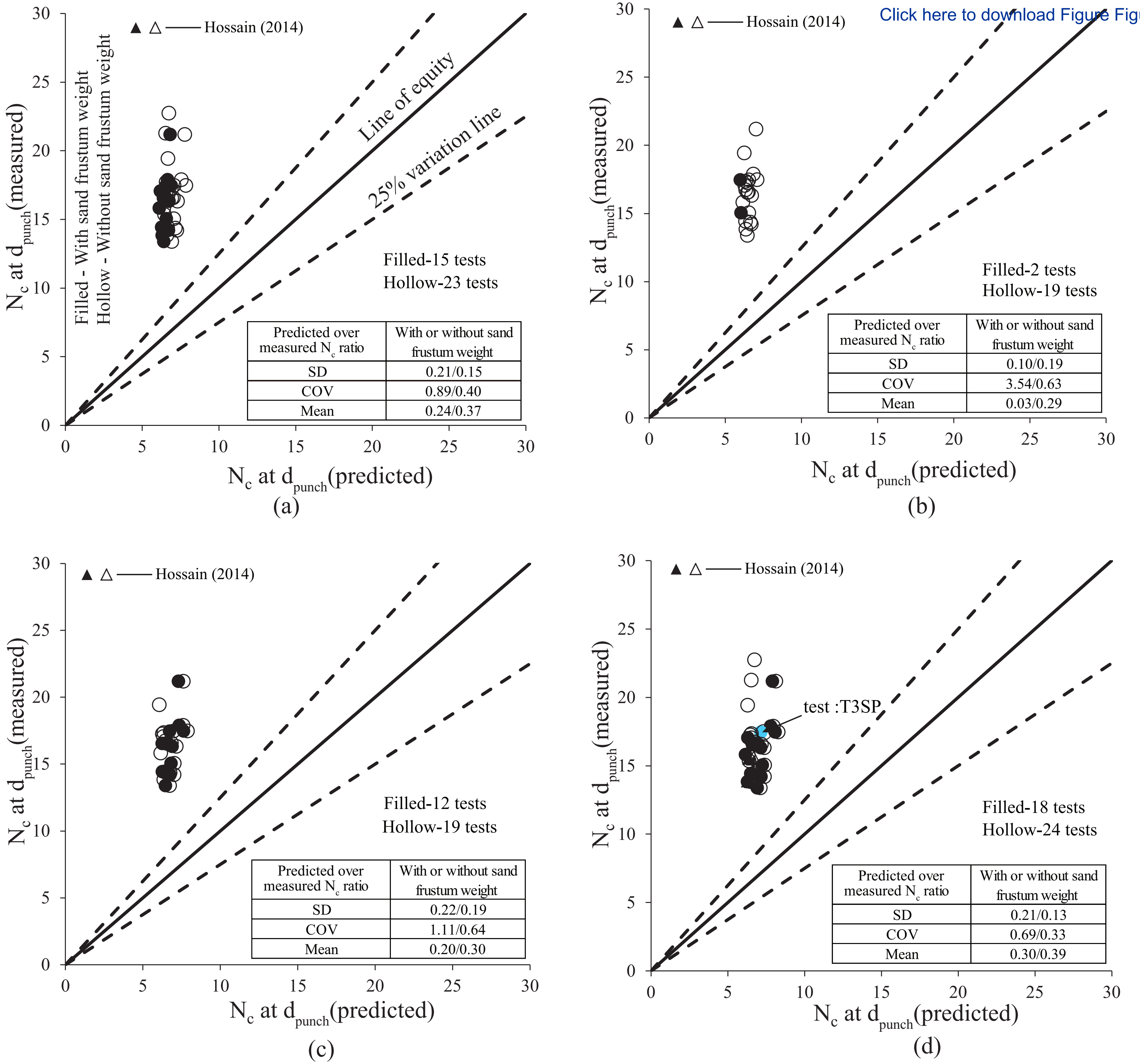

Fig 16

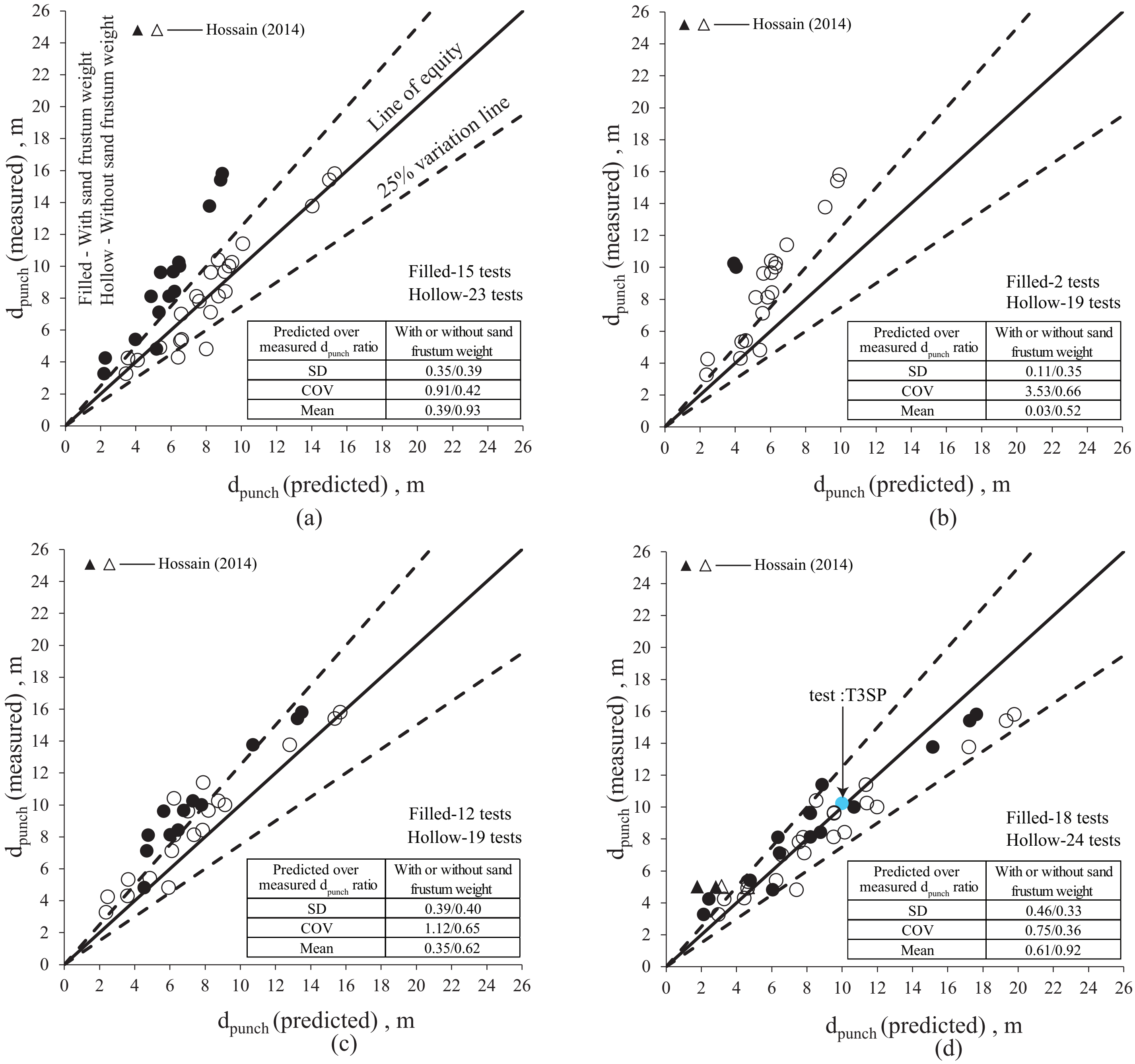
Hossain (2014)
Filled - With sand frustum weight
Hollow - Without sand frustum weight
Line of equity
25% variation line
Filled-15 tests
Hollow-23 tests
Predicted over measured d punch ratio | With or without sand frustum weight
SD | 0.35/0.39
COV | 0.91/0.42
Mean | 0.39/0.93
d punch (measured) , m
d punch (predicted) , m
(a)
Hossain (2014)
Filled-2 tests
Hollow-19 tests
Predicted over measured d punch ratio | With or without sand frustum weight
SD | 0.11/0.35
COV | 3.53/0.66
Mean | 0.03/0.52
(b)
Hossain (2014)
Filled-12 tests
Hollow-19 tests
Predicted over measured d punch ratio | With or without sand frustum weight
SD | 0.39/0.40
COV | 1.12/0.65
Mean | 0.35/0.62
(c)
Hossain (2014)
test :T3SP
Filled-18 tests
Hollow-24 tests
Predicted over measured d punch ratio | With or without sand frustum weight
SD | 0.46/0.33
COV | 0.75/0.36
Mean | 0.61/0.92
(d)

Table 1: Foundation prototype geometries at 200g.

Type of foundation	D * (m)	d_s*(m)	t1* (m)	t2* (m)	t3 * (m)	t (m)
Spudcan (Visualising)	6	1.35	0.86	1.40	0.35	0.15
Flat (Visualising)	6	1.35	-	-	-	1.0
Spudcan (Non-visualising)	6	2.92	0.86	1.40	0.35	0.30
	8	2.92	1.15	1.87	0.58	0.30
	10	2.92	1.44	2.33	0.81	0.30
	12	2.92	1.44	2.80	1.07	0.30
	14	2.92	2.02	3.27	1.27	0.30
	16	2.92	2.30	3.73	1.50	0.30
Flat (Non-visualising) : Cylindrical curvature on underside of 420 mm radius	6	2.92	-	-	-	0.55
	12	2.92	-	-	-	1.19
	16	2.92	-	-	-	1.42

* The geometric parameters D, d_s, t1, t2 & t3 are defined in Figure 2.

Table 2: Details of test geometries and soil properties (all tests conducted at 200 g).

Test*	H_{ct} (m)	H_s (m)	D (m)	H_{ct}/D (-)	H_s/D (-)	s_{um} (kPa)	ρ_{ct} (kPa/m)	s_{ubi} (kPa)	ρ_{cb} (kPa/m)	φ_{cv} (°)	I_D (%)	γ'_s (kN/m^3)	γ'_{ct}** (kN/m^3)	γ'_{cb}** (kN/m^3)	υ (mm/s)	Remarks
T1SP	2.38	4	6	0.40	0.67	4.9	1.9	25.6	2.5	31	74	10.6	6.85	7.32	0.254	PIV visualising tests
T2SP	4.32	4	6	0.72	0.67	4.5	1.6	27	2.5	31	74	10.6	6.85	7.32	0.254	
T3SP	5.47	4	6	0.91	0.67	4.1	1.5	26	2.3	31	74	10.6	6.85	7.32	0.254	
T4SP	0	4	6	0.00	0.67	0	0	18.7	2	31	74	10.6	6.85	7.32	0.254	
T5SP	3.44	2	6	0.57	0.33	4.7	1.7	18.2	2	31	74	10.6	6.85	7.32	0.254	
T6SP	4.35	6	6	0.72	1.00	4.5	1.6	26	2.3	31	74	10.6	6.85	7.32	0.254	
T1FL	2.35	4	6	0.39	0.67	4.9	1.9	25.6	2.5	31	74	10.6	6.85	7.32	0.254	
T2FL	4.01	4	6	0.67	0.67	4.5	1.6	26.7	2.5	31	74	10.6	6.85	7.32	0.254	
T3FL	5.10	4	6	0.85	0.67	4.1	1.5	25.8	2.3	31	74	10.6	6.85	7.32	0.254	
T4FL	0	4	6	0.00	0.67	0	0	18.7	2	31	74	10.6	6.85	7.32	0.254	
T5FL	3.36	2	6	0.56	0.33	4.8	1.7	18.1	2	31	74	10.6	6.85	7.32	0.254	
T6FL	4.05	6	6	0.68	1.00	4.5	1.6	26	2.3	31	74	10.6	6.85	7.32	0.254	
SPa16	6.42	6.25	16	0.40	0.39	0.2	0.5	22.6	2.2	31	51	10.14	6.61	7.63	0.095	Full drum tests: Section-a
SPa14	6.42	6.25	14	0.46	0.45	0.2	0.5	22.6	2.2	31	51	10.14	6.61	7.63	0.109	
SPa12	6.42	6.25	12	0.54	0.52	0.2	0.5	22.6	2.2	31	51	10.14	6.61	7.63	0.127	
SPa10	6.42	6.25	10	0.64	0.63	0.2	0.5	22.6	2.2	31	51	10.14	6.61	7.63	0.152	
SPa6	6.42	6.25	6	1.07	1.04	0.2	0.5	22.6	2.2	31	51	10.14	6.61	7.63	0.254	
FLa6	6.42	6.25	6	1.07	1.04	0.2	0.5	22.6	2.2	31	51	10.14	6.61	7.63	0.254	
SPb16	6.32	4	16	0.39	0.25	0.2	0.5	24.6	2.4	31	51	10.14	6.61	7.63	0.095	Full drum tests: Section-b
SPb12	6.32	4	12	0.53	0.33	0.2	0.5	24.6	2.4	31	51	10.14	6.61	7.63	0.127	
SPb8	6.32	4	8	0.79	0.50	0.2	0.5	24.6	2.4	31	51	10.14	6.61	7.63	0.190	
SPb6	6.32	4	6	1.05	0.67	0.2	0.5	24.6	2.4	31	51	10.14	6.61	7.63	0.254	
FLb12	6.32	4	12	0.53	0.33	0.2	0.5	24.6	2.4	31	51	10.14	6.61	7.63	0.127	
SPc16	4	4	16	0.25	0.25	0.3	0.58	23	2.5	31	51	10.14	6.61	7.63	0.095	Full drum tests: Section-c
SPc8	4	4	8	0.50	0.50	0.3	0.58	23	2.5	31	51	10.14	6.61	7.63	0.190	
SPc6	4	4	6	0.67	0.67	0.3	0.58	23	2.5	31	51	10.14	6.61	7.63	0.254	
FLc16	4	4	16	0.25	0.25	0.3	0.58	23	2.5	31	51	10.14	6.61	7.63	0.095	

* SP=Spudcan; FL=Flat; a, b, c represents the three sections of the drum centrifuge respectively; ** based on average moisture content